Published for SISSA by Springer

Received: October 3, 2025
Revised: December 17, 2025
Accepted: December 18, 2025
Published: February 4, 2026

Z-boson quantum tomography at next-to-leading order

Morgan Del Gratta,[a,b] **Federica Fabbri**,[c,d] **Michele Grossi**,[e] **Fabio Maltoni**,[c,d,e,f] **Davide Pagani**,[d] **Giovanni Pelliccioli**[g,h,*] **and Alessandro Vicini**[a,b]

[a] *Dipartimento di Fisica, Università degli Studi di Milano, Via Celoria 16, I-20133 Milano, Italy*
[b] *INFN, Sezione di Milano, Via Celoria 16, I-20133 Milano, Italy*
[c] *Dipartimento di Fisica e Astronomia, Università di Bologna, Via Irnerio 46, I-40126 Bologna, Italy*
[d] *INFN, Sezione di Bologna, Via Irnerio 46, I-40126 Bologna, Italy*
[e] *European Organization for Nuclear Research (CERN), Esplanade des Particules 1, CH-1211 Geneva 23, Switzerland*
[f] *Centre for Cosmology, Particle Physics and Phenomenology (CP3), Université Catholique de Louvain, 2 Chemin du Cyclotron, B-1348 Louvain-la-Neuve, Belgium*
[g] *Dipartimento di Fisica, Università di Milano-Bicocca, Piazza della Scienza 3, I-20126 Milano, Italy*
[h] *INFN, Sezione di Milano-Bicocca, Piazza della Scienza 3, I-20126 Milano, Italy*

E-mail: morgan.delgratta@unimi.it, federica.fabbri@cern.ch, michele.grossi@cern.ch, fabio.maltoni@unibo.it, davide.pagani@bo.infn.it, giovanni.pelliccioli@unimib.it, alessandro.vicini@mi.infn.it

Abstract: We investigate the origin of the unusually large electroweak (EW) radiative effects observed in the extraction of the spin-density matrix and related observables at colliders, focusing on leptonic Z-boson decays. We compute the Z-boson decay spin-density matrix at next-to-leading order (NLO) and find that, while its analytic structure remains essentially unchanged with respect to leading order, the EW corrections induce a sizeable -35% shift in the spin-analysing power parameter η_ℓ. This effect alone accounts for the striking size of the corrections. For boosted Z bosons, we further show that the treatment of photon radiation in lepton-dressing algorithms significantly affects the extraction of spin-density-matrix coefficients at NLO and must be carefully controlled. To address these challenges, we propose a quantum tomography procedure that is applicable to any final state with one or more on-shell Z bosons that is robust under higher-order corrections. We illustrate its validity and limitations in $pp \to ZZ \to 4\ell$ and in heavy ($M_H > 2M_Z$) Higgs boson decay $H \to ZZ \to 4\ell$.

Keywords: Higher Order Electroweak Calculations, Higgs Properties

ArXiv ePrint: 2509.20456

*Corresponding author.

https://doi.org/10.1007/JHEP02(2026)056

Contents

1 Introduction

The growing interest in accessing quantum-information inspired observables at collider energies [1, 2], also spurred by the recent ATLAS and CMS observation of the entanglement between the spin of top-quarks [3–5], has triggered numerous studies in other channels, amongst which a significant role is played by final states with two electroweak (EW) bosons in the final state [6–28]. A central tool for accessing quantum-inspired observables related to the spin of particles produced at colliders is the *quantum tomography* (QT) procedure. This method enables the reconstruction of the full or partial spin-density matrix, which encapsulates the polarisation and spin-correlation information of the system. For example, the case of a pair of massive electroweak bosons can be thought of as a two-qutrit system, i.e., a bipartite quantum system composed of two three-level subsystems. In the most general case, such a system is characterised by eighty independent polarisation and spin-correlation coefficients, whose values are sensitive to the underlying production dynamics. QT provides a systematic framework to extract these coefficients by analysing the angular distributions of the bosons decay products; see e.g. ref. [1].

The standard QT procedure is based on leading order (LO) computations of scattering amplitudes. However, the data that are being collected at the LHC include also effects due to higher-order corrections, both loop and real radiation, in the QCD and EW couplings. It is therefore mandatory to study the impact that such higher order effects may have on the extracted spin density matrix. The first studies of such corrections in the context of two-boson spin correlations at colliders, i.e. systems of two qutrits in the quantum-information wording,

JHEP02(2026)056

are very recent [17, 23, 25, 26, 28]. It has been shown for Higgs-boson decays to four charged leptons [17, 23, 26] that higher-order and off-shell effects induce very large corrections, making the spin-density matrix for two-qutrit systems not well-defined and its interpretation in terms of spin entanglement and Bell-inequality violation possibly problematic. This issue arises from large corrections to the spin analysing power η_ℓ, a key quantity that relates the spin of the parent particle to the directions of the decay products and enters in the extraction of the coefficients of the spin density matrix. This problem is particularly severe in the $Z \to \ell^+\ell^-$ process due to the small η_ℓ value in this process. The first insightful proposal to solve the problem has been made in ref. [26], where it was noted that the large part of NLO EW effects could be incorporated at LO via a change of scheme, i.e. using $\sin^2\theta_{\rm w}^{\rm eff}$ [29–36].

In this work we further investigate and fully understand the effects of the radiative EW corrections on the QT procedure for Z bosons decays and propose a general solution.

First, we perform the complete calculation at next-to-leading-order (NLO) of all entries of the decay spin-density matrix for a Z boson decaying into two charged leptons. Via a numerical analysis, we prove that the LO analytic structure of the decay matrix is not changed when considering NLO EW effects and relying on dressed charged leptons, up to a sizeable modification that can be fully absorbed into the spin-analysing power. This allows us to fully generalise the approach to any process involving an arbitrary number of on-shell Z bosons in the final state, such as double and triple vector boson production, associated production, tZ, $t\bar{t}$Z and so on.

Second, we show how the derived decay-only results can be consistently applied also to the case where final state Z bosons are boosted. In such a situation, the details of the lepton-dressing algorithm affect the evaluation of the spin-analysing power and make the extraction of the spin-density matrix coefficients rather delicate at NLO. Employing a pole-approximation strategy and selecting helicity states in tree-level and one-loop amplitudes, we derive a sound prescription to perform a QT of two-qutrit systems that is correct at NLO EW and systematically improvable at higher orders.

Third, we show how in the case of the Higgs decay into two Z bosons, subsequently decaying into leptons, the fact that one of the two Z must be off-shell affects the aforementioned prescription, which instead would still be valid for a heavier Higgs with $M_{\rm H} \gg 2M_{\rm Z}$. Such academic scenario is also exploited in order to show how effects formally of higher order (NNLO EW) and corresponding to NLO EW corrections to both decays are sizeable and we support our prescription for the extraction of the coefficients of the ZZ spin density matrix.

The paper is organised as follows. In section 2 we formally introduce the problem and define relevant quantities at LO and NLO EW accuracy. In section 3.1 we consider the decay of a Z boson (in its rest frame) and show how EW radiative effects modify the diagonal and off-diagonal entries of the decay matrix. The effects of the lepton-dressing algorithm, in association with cuts at production level in LHC processes are discussed in section 3.2, exploiting the helicity-amplitude method. In section 4 we discuss in detail the structure of NLO EW corrections in the production + decay process for the ZZ production. We compare results obtained via QT and helicity-amplitude methods for quantum-information observables at LO and NLO EW accuracy. We derive via this comparison the correct prescription that should be employed in the case of QT. In section 5 we discuss the case of the Higgs decay,

JHEP02(2026)056

for which problems persists, and we further support our prescription for the case of ZZ production and a possible heavier Higgs, highlighting the relevance of higher-order corrections. In section 6 we draw our conclusions and provide an outlook.

2 Quantum tomography and helicity amplitudes

In quantum mechanics, the spin-density matrix of a multipartite system composed of arbitrary-spin (qudit) states encodes its most general quantum spin configuration, whether pure or mixed. In particle physics, fermions and massless bosons correspond to qubits, while massive vector bosons such as the W and Z act as qutrits. It is therefore of interest to study quantum correlations among final states produced in high-energy collisions, which can be computed perturbatively from first principles using QFT and in the present case, the Standard Model (SM) Lagrangian. Because the physical massive vector bosons are unstable and decay well before their propagation can be directly measured in the detector, only the momenta of their decay products can be observed. The final spin state of each boson, and of the composite system as a whole, must therefore be inferred statistically from the distributions of decay products. This procedure relies on several assumptions. The first is that the EW bosons are on their mass shell. This can be enforced by selecting events in which the invariant mass of the decay products matches the mass of the corresponding bosons. From a theoretical perspective, this condition allows the amplitude to be factorised into production and decay parts and ensures that a well-defined spin-density matrix can be determined to all orders in perturbation theory. Experimentally, however, reconstructing the spin of the original vectors from the directions of their decay products introduces complications. An obvious issue is the possible presence of additional radiation in the event. First, one must identify whether this radiation originates from the production or the decay process, a task that can be performed unambiguously only if the energy of the radiation is larger than the width of the decaying particle. In addition, it requires using the invariant-mass condition, something that can be done only if the detector has excellent energy-momentum resolution. Finally, in the case of final-state radiation, its contribution must be correctly incorporated into the tomography procedure. Moreover, when comparing theory with experiment, higher-order virtual effects must also be included when relevant. A robust procedure that enables the reliable reconstruction of the overall spin-density state of the heavy system and its comparison with theoretical predictions is therefore essential. In this section we introduce and compare two complementary approaches to extracting the spin-density matrix of a pair of EW bosons decaying into a four-lepton final state, with inclusiveness over additional radiation (in the present case, QED). Both methods — Quantum Tomography (QT) and Helicity Amplitudes (HA) — assume, explicitly or implicitly, that the process is dominated by two on-shell spin-1 bosons, yet they offer distinct perspectives.

QT defines a finite set of observables over the full phase space by projecting onto the elements of a spherical-harmonics basis of rank ≤ 2, whose coefficients are directly related to the spin-density matrix. While this definition can always be applied to experimental data, interpreting the results requires care. Practical limitations such as incomplete phase-space coverage from fiducial or selection cuts, the presence of real radiation, and non-resonant

JHEP02(2026)056

contributions may invalidate the assumption that a few spherical harmonics suffice. In current analyses, the data are unfolded but interpreted through a leading-order (LO) calculation.

The HA method computes the cross sections for each helicity configuration of the intermediate bosons, providing direct control over the contribution of every spin state to the total cross section and hence to the spin-density matrix. Decay kinematics and additional quantum effects are incorporated separately for each helicity, yielding a more explicit link between theoretical predictions and experimental measurements.

Although the two approaches are equivalent at LO, their behaviour differs once higher-order corrections are included. A comparison at next-to-leading order (NLO) therefore quantifies the respective advantages and limitations, guiding the choice of the most accurate strategy to determine the spin-density matrix. We now start by presenting the elements and methods proper of a LO analysis and then at move to NLO.

2.1 Leading order

If we consider the $\mathrm{Z}+X$ production process, with the Z boson decaying into two fermions, at LO and assuming the strict narrow-width-approximation (NWA), i.e. forcing the Z boson to be on-shell, the angular distribution of one of the fermions can be written as

$$\frac{4\pi}{3}\frac{1}{\sigma}\frac{\mathrm{d}^2\sigma}{\mathrm{d}\cos\theta\,\mathrm{d}\phi} = \sum_{\lambda,\lambda'}\rho_{\lambda,\lambda'}\Gamma_{\lambda,\lambda'}(\theta,\phi)\,, \tag{2.1}$$

where σ is the total cross section, ρ is the spin-density matrix of the $\mathrm{Z}+X$ system traced over the spin-indices of X, and Γ is the spin-density decay matrix of the Z, which depends on the polar (θ) and the azimuthal (ϕ) decay angles of one of the two fermions in the corresponding Z-boson rest frame. In the following, for simplicity, we will refer to Γ as the "decay matrix" and we will consider the leptonic decay $\mathrm{Z}\to\ell^+\ell^-$, where θ and ϕ refer to the positively charged lepton ℓ^+ in the Z-boson rest frame. The indices $\lambda,\lambda'=0,1,-1$ label the physical polarisation states associated to the Z boson (longitudinal, left- and right-handed). When also the other particles produced in association with the Z are considered and their spin-indices are not traced, eq. (2.1) can exhibit the full form of the spin-density matrix. For instance, in the case of the ZZ bipartite qutrit system, with both Z bosons decaying leptonically, one obtains

$$\frac{16\pi^2}{9}\frac{1}{\sigma}\frac{\mathrm{d}^4\sigma}{\mathrm{d}\cos\theta_1\,\mathrm{d}\phi_1\,\mathrm{d}\cos\theta_2\,\mathrm{d}\phi_2} = \sum_{\lambda_1,\lambda_1',\lambda_2,\lambda_2'}\rho_{\lambda_1,\lambda_1',\lambda_2,\lambda_2'}\Gamma_{\lambda_1,\lambda_1'}(\theta_1,\phi_1)\Gamma_{\lambda_2,\lambda_2'}(\theta_2,\phi_2)\,, \tag{2.2}$$

where the subscripts 1 and 2 label the quantities associated to the two Z bosons.[1]

At LO and assuming NWA, the spin-density matrix can be extracted in two different manners:

- QT: via the angular distributions of the positively[2] charged leptons it is possible to reconstruct the spin-density matrix. In short, by projecting the angular distributions onto spherical harmonics $Y_{lm}(\theta,\phi)$, it is possible to derive the individual entries of ρ.

[1] Note that in this work we consider final state fermions in the two decays distinguishable, i.e., we choose different flavours. While this constraint can be lifted, it simplifies the discussion in the following and most of the time is not relevant. We will further comment on this when necessary.

[2] The use of the negatively charged leptons yields equivalent results, up to an overall sign flip in the entries sensitive to η_ℓ.

JHEP02(2026)056

- HA: the individual quantities $\rho_{\lambda,\lambda'}$ and $\Gamma_{\lambda,\lambda'}$ entering eq. (2.1) can be computed either separately or with contracted helicity indices, depending on the on-shell approximation used for the calculation. More generally, the same argument can be repeated for the case of the density matrix of a bipartite ZZ system, as in eq. (2.2).

It is clear that at LO, assuming NWA and imposing no cuts on the lepton momenta, the calculation of ρ via QT or HA leads to exactly the same results. For a generic $\mathrm{Z}+X$ system, following the notation of ref. [17], eq. (2.1) can be written as

$$\frac{1}{\sigma}\frac{\mathrm{d}\sigma}{\mathrm{d}\cos\theta\,\mathrm{d}\phi} = \frac{1}{4\pi} + \sum_{l=1}^{2}\sum_{m=-l}^{l} \alpha_{lm}\, Y_{lm}(\theta,\phi)\,, \tag{2.3}$$

and for the particular case of a ZZ pair, eq. (2.2) can be written as

$$\begin{aligned}\frac{1}{\sigma}\frac{\mathrm{d}\sigma}{\mathrm{d}\cos\theta_1\,\mathrm{d}\phi_1\,\mathrm{d}\cos\theta_2\,\mathrm{d}\phi_2} = \frac{1}{(4\pi)^2} &+ \frac{1}{4\pi}\sum_{l=1}^{2}\sum_{m=-l}^{l} \alpha^{(1)}_{lm}\, Y_{lm}(\theta_1,\phi_1) \\ &+ \frac{1}{4\pi}\sum_{l=1}^{2}\sum_{m=-l}^{l} \alpha^{(2)}_{lm}\, Y_{lm}(\theta_2,\phi_2) \\ &+ \sum_{l=1}^{2}\sum_{l'=1}^{2}\sum_{m=-l}^{l}\sum_{m'=-l'}^{l'} \gamma_{lml'm'}\, Y_{lm}(\theta_1,\phi_1)\, Y_{l'm'}(\theta_2,\phi_2)\,,\end{aligned} \tag{2.4}$$

with the decay angles computed w.r.t some reference axis, the spin-quantisation axis, which in this work we choose to be the so-called *modified helicity coordinate system* [37].[3] Since $Y_{lm}(\theta_i,\phi_i)$ are an orthogonal basis, it is possible to extract the α and γ coefficients by projecting the angular distributions on them.

Since the analytic structure of both the decay density matrix Γ and the spin-density matrix ρ are known at LO, it is possible to extract from the α_{lm} and $\gamma_{lml'm'}$ coefficients the entries of ρ. In particular, the QT approach relies on the LO-accurate Z-boson decay matrix [38, 39],

$$\Gamma(\theta,\phi) = \frac{1}{4}\begin{pmatrix} 1+2\eta_\ell\cos\theta+\cos^2\theta & \sqrt{2}\,\sin\theta(\eta_\ell+\cos\theta)e^{\mathrm{i}\phi} & (1-\cos^2\theta)e^{2\mathrm{i}\phi} \\ \sqrt{2}\,\sin\theta(\eta_\ell+\cos\theta)e^{-\mathrm{i}\phi} & 2\,(1-\cos^2\theta) & \sqrt{2}\,\sin\theta(\eta_\ell-\cos\theta)e^{\mathrm{i}\phi} \\ (1-\cos^2\theta)e^{-2\mathrm{i}\phi} & \sqrt{2}\,\sin\theta(\eta_\ell-\cos\theta)e^{-\mathrm{i}\phi} & 1-2\eta_\ell\cos\theta+\cos^2\theta \end{pmatrix}. \tag{2.5}$$

The quantity η_ℓ in eq. (2.5) is the so called spin-analysing power,[4] which for massless charged leptons in Z decays reads, at LO,

$$\eta_\ell = \frac{2\,g_{V,\ell}\,g_{A,\ell}}{g^2_{V,\ell}+g^2_{A,\ell}} = \frac{1-4\sin^2\theta_\mathrm{w}}{1-4\sin^2\theta_\mathrm{w}+8\sin^4\theta_\mathrm{w}} = 0.2131\ldots\,, \tag{2.6}$$

with the input parameter that are listed in section 3.1 and with $g_{V,\ell}$, $g_{A,\ell}$ being respectively the vector and axial-vector coupling of the Z boson to leptons. This parameter has been

[3] It defines the reference axis as the spatial direction of the boson V_1 in the centre-of-mass frame of the di-boson system V_1V_2. This choice implies that the polarisations and spin correlations are defined in the centre-of-mass frame of the di-boson system.

[4] The parameter η_ℓ in this work is equivalent to $-\alpha_\ell$ in ref. [23].

JHEP02(2026)056

widely investigated at LEP through asymmetries [40], and as already mentioned in the introduction, it is the culprit of the giant EW corrections appearing in QT with Z bosons that decay leptonically. It receives large corrections since the $(1 - 4\sin^2\theta_{\rm w})$ factor is small due to an accidental cancellation.

In quantum mechanics the ρ matrix for a two-qutrit system can be conveniently written in terms of the irreducible tensorial representations T_{lm} of the boson spin [7], whose explicit form is shown in appendix A,

$$\rho = \frac{1}{9}\left[\mathbf{1}_3 \otimes \mathbf{1}_3 + A^{(1)}_{lm}(T_{lm} \otimes \mathbf{1}_3) + A^{(2)}_{lm}(\mathbf{1}_3 \otimes T_{lm}) + C_{lml'm'}(T_{lm} \otimes T_{l'm'})\right]. \tag{2.7}$$

The different symmetries of the system determine which of the A and C coefficients are non-vanishing and the relations amongst them [23]. In particular, knowing all the A and C coefficients, the whole ρ matrix can be reconstructed.

Using the same basis, the decay matrix Γ in eq. (2.5) can also be rewritten as

$$\Gamma = \frac{1}{3}\left[\mathbf{1}_3 + \sqrt{2\pi}\,\eta_\ell\, T_{1m}Y_{1m} + \sqrt{\frac{2\pi}{5}}\,T_{2m}Y_{2m}\right]. \tag{2.8}$$

Plugging eqs. (2.7) and (2.8) into eq. (2.2) it is possible to derive an expression of the same form of eq. (2.4) (see e.g. ref. [23] for more details) and derive relations between the coefficients α, γ and A, C:

$$\begin{aligned}
&\sqrt{8\pi}\alpha_{1m} = \eta_\ell\, A_{1m}, \qquad \sqrt{40\pi}\alpha_{2m} = A_{2m}, \qquad 8\pi\gamma_{1m1m'} = \eta_\ell^2\, C_{1m1m'},\\
&40\pi\gamma_{2m2m'} = C_{2m2m'}, \qquad 8\pi\sqrt{5}\gamma_{2m1m'} = \eta_\ell\, C_{2m1m'}, \qquad 8\pi\sqrt{5}\gamma_{1m2m'} = \eta_\ell\, C_{1m2m'}.
\end{aligned} \tag{2.9}$$

Thus, at LO and assuming NWA, it is possible via QT to extract α and γ coefficients and, since Γ is known, convert them to A and C coefficients and in turn the entries of ρ. The exact same results would be obtained via the HA, calculating directly $\rho_{\lambda_1,\lambda_1',\lambda_2,\lambda_2'}\Gamma_{\lambda_1,\lambda_1'}(\theta_1,\phi_1)\Gamma_{\lambda_2,\lambda_2'}(\theta_2,\phi_2)$ and removing/dividing by the contribution of the Γ's.

Before moving on to the NLO case, we provide some more details on the HA approach. If for a $\mathrm{Z} + X$ production process, with subsequent Z decay, we denote as $\mathcal{A}_{\rm unp}$ the unpolarised amplitude associated to the production $\times$ decay mechanism, this amplitude can be written as a sum of physical-helicity amplitudes [41]:

$$\mathcal{A}_{\rm unp} = \mathcal{A}^{(\rm prod)}_{\mu}\,\frac{\sum_\lambda \varepsilon^{*\,\mu}_\lambda \varepsilon_\lambda{}^{\nu}}{k_{\rm Z}^2 - M_{\rm Z}^2 + {\rm i}M_{\rm Z}\Gamma_{\rm Z}}\,\mathcal{A}^{(\rm dec)}_{\nu} = \sum_\lambda \frac{\mathcal{A}^{(\rm prod)}_\lambda \mathcal{A}^{(\rm dec)}_\lambda}{k_{\rm Z}^2 - M_{\rm Z}^2 + {\rm i}M_{\rm Z}\Gamma_{\rm Z}} \equiv \sum_\lambda \mathcal{A}_\lambda\,, \tag{2.10}$$

where $k_{\rm Z}$, $M_{\rm Z}$ and $\Gamma_{\rm Z}$ are the four momentum, the pole mass and the pole width of the Z boson, respectively. In doing so we have just assumed the intermediate Z boson in the s-channel and that $A^{(\rm prod)}$ and $A^{(\rm dec)}$ are evaluated with $k_{\rm Z}^2 = M_{\rm Z}^2$, as done in the pole approximation (PA) [41–57]. The amplitude $\mathcal{A}_{\rm unp}$ can therefore be factorised, helicity by helicity, into a production amplitude $\mathcal{A}^{(\rm prod)}_\lambda$ and a decay amplitude $\mathcal{A}^{(\rm dec)}_\lambda$, possibly taking into account off-shell effects in the denominator of the propagator. The NWA approximation is simply obtained in the $\Gamma_{\rm Z}/M_{\rm Z} \to 0$ limit, after $k_{\rm Z}^2$ integration.[5]

[5] In the literature, the NWA can also consists of a off-shell reshuffling of the amplitude evaluated on-shell [58–62]. In this paper we will refer to NWA as strictly on-shell. We note that anyway, also taking into account off-shell effects, it is not equivalent to the pole expansion, see e.g. ref. [63].

JHEP02(2026)056

Squaring eq. (2.10), we obtain

$$|\mathcal{A}_{\text{unp}}|^2 = \left|\sum_\lambda \mathcal{A}_\lambda\right|^2 \propto \sum_{\lambda,\lambda'} \left(\mathcal{A}_\lambda^{(\text{prod})*}\mathcal{A}_{\lambda'}^{(\text{prod})}\right)\left(\mathcal{A}_\lambda^{(\text{dec})*}\mathcal{A}_{\lambda'}^{(\text{dec})}\right) \tag{2.11}$$

where in the NWA, besides normalisation constants, $\mathcal{A}_\lambda^{(\text{prod})*}\mathcal{A}_{\lambda'}^{(\text{prod})}$ and $\mathcal{A}_\lambda^{(\text{dec})*}\mathcal{A}_{\lambda'}^{(\text{dec})}$ respectively correspond to $\rho_{\lambda,\lambda'}$ and $\Gamma_{\lambda,\lambda'}$ in eq. (2.1). More in detail, if we call σ^{prod} the unpolarised cross section for the production of the $\text{Z} + X$ process, so calculated via $\left|\sum_\lambda \mathcal{A}_\lambda^{(\text{prod})}\right|^2$, and instead $\sigma^{\text{prod}}_{\lambda,\lambda'}$ if calculated via $\left(\mathcal{A}_\lambda^{(\text{prod})*}\mathcal{A}_{\lambda'}^{(\text{prod})}\right)$, then

$$\rho_{\lambda,\lambda'} = \frac{\sigma^{\text{prod}}_{\lambda,\lambda'}}{\sigma^{\text{prod}}}\,. \tag{2.12}$$

This definition can be easily extended in the case of multiple Z bosons, as in the case of eq. (2.2). Analogously, if we call σ^{dec} the unpolarised decay width for the $\text{Z} \to \ell^+\ell^-$, so calculated via $\left|\sum_\lambda \mathcal{A}_\lambda^{(\text{dec})}\right|^2$, and $\sigma^{\text{dec}}_{\lambda,\lambda'}$ when it is calculated via $\left(\mathcal{A}_\lambda^{(\text{dec})*}\mathcal{A}_{\lambda'}^{(\text{dec})}\right)$, then

$$\Gamma_{\lambda,\lambda'} = \frac{\sigma^{\text{dec}}_{\lambda,\lambda'}}{\sigma^{\text{dec}}}\,. \tag{2.13}$$

In conclusion, via the HA method, each term entering in the sum of the r.h.s. of eq. (2.11) can be computed, and the $\rho_{\lambda,\lambda'}$ can be either calculated directly or extracted by the HA by simply dividing by the corresponding $\Gamma_{\lambda,\lambda'}$. This is particularly convenient when acceptance or selection cuts on the final states need to be taken into account, as done in sections 3.2 and 4. The same applies to an arbitrary number of intermediate EW bosons.

In general, the HA method can be used for the calculation of integrated and differential polarised cross sections. In the case of Z-boson pairs, it has already been applied up to NLO EW + NNLO QCD accuracy as well as in the presence of parton-shower-matching and multi-jet-merging effects [63]. In principle, each component $\mathcal{A}_\lambda^{(\text{prod})}$ and $\mathcal{A}_\lambda^{(\text{dec})}$ can be independently calculated. In practice, as already mentioned, most of the available MC tools evaluate $\mathcal{A}_\lambda$, such that cuts can directly be taken into account at the production $\times$ decay level.

2.2 Next-to-leading order

As already discussed in the introduction, the extraction via QT of the coefficients of the spin-density matrix in the presence of leptonically decaying Z bosons is plagued by large EW corrections [17]. They emerge from the decay matrix Γ and are erroneously propagated onto the spin-density matrix ρ [23] if in the relation between $\gamma_{1m1m'}$ and $C_{1m1m'}$ in eq. (2.9) the LO value of the spin-analysing power η_ℓ is employed. In ref. [26] it has been shown that by simply replacing in the definition of η_ℓ in eq. (2.6) the NLO EW corrected value of the EW mixing angle, $\sin^2\theta_{\text{w}}^{\text{eff}}$, the difference between $C_{1m1m'}$ coefficients obtained at LO and NLO diminishes. Still, the consistency of this procedure has to be better understood and validated.

In the NWA or PA, via the HA method, eq. (2.1) can be calculated at NLO EW accuracy and, by construction, it preserves the factorised form that is present in the r.h.s. of the equation. This means that both the decay matrix Γ and the ρ spin-density matrix can

JHEP02(2026)056

be separately calculated at NLO EW accuracy. Thus, it is possible to check under which conditions the extraction of the ρ spin-density matrix via QT returns the same values obtained via the HA method. In other words, when the QT-extracted value corresponds to the "true" value. In practice, in the case of QT, the NLO EW corrections are evaluated to the full process of production and decay. The requirement to use the PA or the NWA is not present and also non-resonant effects can be calculated. With QT, the coefficients α and γ are directly calculated via the momenta of the final-state leptons and converted to A and C and in turn to the entries of ρ. We stress that a specific assumption on the value of η_ℓ has to be taken for performing such conversion. On the contrary, via the HA method the workflow is the opposite. The entries of ρ are directly calculated, the A and C coefficients are derived from them and then converted to the α and γ ones via the computed value of η_ℓ.

The HA method directly gives access to the spin-density matrix of the $\mathrm{Z} + X$ system, but it is a purely calculation method and by construction cannot account for contributions that do not feature intermediate resonating Z boson, which instead can be present for the final state $\ell^+\ell^- + X$. On the contrary, the QT is applied directly on the $\ell^+\ell^- + X$ final state, and therefore the NLO EW calculation can be performed in any approximation, however in the extraction of the A and C coefficients the intermediate Z must be assumed and the value of η_ℓ must also be chosen properly. The comparison of the two methods precisely helps in this choice, and at the same time allows one to investigate effects related to non-resonant contributions or other features of the set-up considered, such as cuts. Especially in the context of the SM Higgs boson decay into four leptons, we will see in section 5 the relevance of such comparison.

It is worth to remind the reader that so far the QT has not been exploited at the experimental level to extract the complete spin-density matrix in diboson final states from LHC data. However, this technique has been applied by the CMS Collaboration in top-quark pair final states to determine the corresponding spin density matrix elements [5]. In the case of diboson processes, the polarisation fractions have been extracted from LHC Run-2 data via polarisation-template fits [37, 64–69]. These experimental results rely on helicity-dependent theoretical predictions (polarisation templates) obtained with the HA method tailored to the 9 diagonal (azimuthal-averaged) entries of the spin-density matrix [41, 42, 46–48, 52–55, 57, 60, 62, 63].

To ensure a consistent comparison between QT and HA results, it should be emphasised that the calculation of NLO EW corrections to a cross section includes only the exact $\mathcal{O}(\alpha_{\mathrm{ew}})$ contributions. Higher-order terms, such as $\mathcal{O}(\alpha_{\mathrm{ew}}^2)$ and beyond, are not taken into account. On the other hand, the ρ and the Γ must respectively satisfy the conditions $\mathrm{Tr}(\rho) = 1$ and $\mathrm{Tr}(\Gamma) = 1$, such that both at LO and NLO EW accuracy one has to keep $\mathcal{O}(\alpha_{\mathrm{ew}})$ corrections both in the numerator and the denominator in their definitions (eqs. (2.12) and (2.13)), with no exact expansion. This means that, e.g. , if we consider eq. (2.2), which we rewrite in a compact way as

$$\frac{16\pi^2}{9}\frac{1}{\sigma^{\mathrm{LO}}}\frac{\mathrm{d}^4\sigma^{\mathrm{LO}}}{\mathrm{d}\Omega_1\,\mathrm{d}\Omega_2} = \rho^{\mathrm{LO}}\,\Gamma_1^{\mathrm{LO}}\,\Gamma_2^{\mathrm{LO}}\,, \tag{2.14}$$

JHEP02(2026)056

at NLO EW accuracy, assuming the same factorised structure that is present in eq. (2.10), one obtains

$$\begin{aligned}\frac{16\pi^2}{9}\frac{1}{\sigma^{\rm NLO}}\frac{{\rm d}^4\sigma^{\rm NLO}}{{\rm d}\Omega_1\,{\rm d}\Omega_2} \;=\; & \rho^{\rm LO}\,\Gamma_1^{\rm LO}\,\Gamma_2^{\rm LO} \\ & +\delta\rho^{\rm NLO}\,\Gamma_1^{\rm LO}\,\Gamma_2^{\rm LO} + \rho^{\rm LO}\,\delta\Gamma_1^{\rm NLO}\,\Gamma_2^{\rm LO} + \rho^{\rm LO}\,\Gamma_1^{\rm LO}\,\delta\Gamma_2^{\rm NLO} \\ & +\mathcal{O}(\alpha_{\rm ew}^2)\,,\end{aligned} \tag{2.15}$$

where $\delta\rho^{\rm NLO}$ and $\delta\Gamma_i^{\rm NLO}$ are defined through

$$\rho^{\rm NLO} = \rho^{\rm LO} + \delta\rho^{\rm NLO} + \mathcal{O}(\alpha_{\rm ew}^2)\,, \qquad \Gamma_i^{\rm NLO} = \Gamma_i^{\rm LO} + \delta\Gamma_i^{\rm NLO} + \mathcal{O}(\alpha_{\rm ew}^2)\,. \tag{2.16}$$

In all the previous equations we have dropped the spin indices and we imply the summation over them. The equations are valid both for NWA and double-pole-approximation (DPA), since the additional Breit-Wigner that is present in the latter it is exactly canceled by the $1/\sigma^{\rm NLO}$ normalisation. We want to stress that the $\mathcal{O}(\alpha_{\rm ew}^2)$ term appearing in eq. (2.16) is not related to simultaneous $\mathcal{O}(\alpha_{\rm ew})$ corrections in the production and/or one or more decay entering σ. Such contributions are never present in an NLO EW calculation for the cross section of the production + decay process; they would appear only at NNLO EW or at higher orders.[6] Instead, the $\mathcal{O}(\alpha_{\rm ew}^2)$ term corresponds to contributions that involve at the same time, after the expansion, corrections in the production and in one decay (or in two different decays), but with one contribution coming from the numerator of the l.h.s. of eq. (2.16) and the other one from the denominator. In other words, they depend on the unpolarised production and/or decay. However, if at the unpolarised and inclusive level the NLO corrections are small, as typically it is unless very boosted kinematics are selected, such contributions are negligible in our discussion.

Following the same logic, when η_ℓ is present, the relations that allow for translating the information from angular distributions (α and γ) to the coefficients of the ρ matrix (A and C), see eq. (2.9), are expected to be modified as

$$\sqrt{8\pi}\alpha_{1m}^{\rm NLO} = \eta_\ell^{\rm LO}\,A_{1m}^{\rm LO}\left(1+\frac{\delta\eta_\ell^{\rm NLO}}{\eta_\ell^{\rm LO}}+\frac{\delta A_{1m}^{\rm NLO}}{A_{1m}^{\rm LO}}\right), \tag{2.17}$$

$$8\pi\sqrt{5}\gamma_{1m2m'}^{\rm NLO} = \eta_\ell^{\rm LO}\,C_{1m2m'}^{\rm LO}\left(1+\frac{\delta\eta_\ell^{\rm NLO}}{\eta_\ell^{\rm LO}}+\frac{\delta C_{1m2m'}^{\rm NLO}}{C_{1m2m'}^{\rm LO}}\right), \tag{2.18}$$

$$8\pi\gamma_{1m1m'}^{\rm NLO} = (\eta_\ell^{\rm LO})^2\,C_{1m1m'}^{\rm LO}\left(1+2\frac{\delta\eta_\ell^{\rm NLO}}{\eta_\ell^{\rm LO}}+\frac{\delta C_{1m1m'}^{\rm NLO}}{C_{1m1m'}^{\rm LO}}\right), \tag{2.19}$$

where the same convention already adopted for ρ and Γ has been used in order to denote LO and NLO quantities also for η_ℓ and the A and C coefficients. The main point is that the NLO EW version of each quantity cannot be simply plugged into eq. (2.16) for a consistent comparison between the results obtained via QT or the HA method.

A crucial step is the proper definition of $\eta_\ell^{\rm NLO}$. Consistently with the perturbative expansion, we can write:

$$\eta_\ell = \eta_\ell^{\rm LO} + \delta\eta_\ell^{\rm NLO} + \mathcal{O}(\alpha_{\rm ew}^2) = \eta_\ell^{\rm NLO} + \mathcal{O}(\alpha_{\rm ew}^2)\,.$$

[6] The relevance of these contributions in the comparison with data is precisely the subject of section 5.2.

JHEP02(2026)056

To retain at NLO EW accuracy the same relations between the α, γ and A, C coefficients as at LO, the analytic form of eq. (2.5) must be preserved. If this holds, then $\eta_\ell^{\rm NLO}$ is the corresponding value of the spin analysing power entering the NLO decay matrix. Therefore, the spin analysing power can be obtained by taking the LO definition in eq. (2.6) and directly plugging the value $\sin^2\theta_{\rm w}^{\rm eff}$ computed at NLO EW, i.e. $\eta_\ell^{\rm NLO} = \eta_\ell^{\rm eff}$, where

$$\eta_\ell^{\rm eff} \equiv \eta_\ell^{\rm LO}\Big|_{\sin^2\theta_{\rm w}\to\sin^2\theta_{\rm w}^{\rm eff}} = \frac{1-4\sin^2\theta_{\rm w}^{\rm eff}}{1-4\sin^2\theta_{\rm w}^{\rm eff}+8\sin^4\theta_{\rm w}^{\rm eff}}\,. \tag{2.20}$$

We reckon that $\sin^2\theta_{\rm w}^{\rm eff}$ has been precisely defined for the asymmetries on the Z resonance. However, the fact that the LO analytic structure of the Γ matrix is unaltered at NLO is far from obvious, since the NLO EW corrections also include the real radiation of photons ($\mathrm{Z}\to\ell^+\ell^-\gamma$). The decay matrix could have higher powers in $\cos\theta$ or $e^{i\phi}$, i.e., it could depend on $Y_{lm}(\theta,\phi)$ with $l>2$. If the angular structure of the matrix is significantly altered, the role of η_ℓ itself, as well as how to define it unambiguously, becomes unclear. This is precisely what we investigate in section 3. First in section 3.1 we calculate the decay density matrix Γ at NLO EW accuracy and we check the validity of the approximating it via a LO simulation with $\eta_\ell^{\rm eff}$. Then in section 3.2 we evaluate it, via HA, in realistic processes (production $\times$ decay), taking into account cuts in the laboratory frame.

3 Spin-analysing power at NLO EW

3.1 $\mathrm{Z}\to\ell^+\ell^-$ and the decay matrix

We have applied the HA method introduced in section 2 to carry out the calculation of the 8 independent entries of the NLO EW decay matrix, $\Gamma^{\rm NLO}$, for the inclusive process $\mathrm{Z}\to\ell^+\ell^-(+X)$, which includes also the contributions from the real emission of photons $\mathrm{Z}\to\ell^+\ell^-\gamma$. Such contributions could in principle disrupt the two-body nature of the analytic structure of the entries of eq. (2.5). Representative diagrams entering the calculation, both for real and virtual contributions are shown in figure 1. The calculation has been performed with two fully independent codes:

- (MG5) a private version of MadGraph5_aMC@NLO [70, 71], version 3.3.2, which allows for computing diagonal entries of the decay matrix at NLO EW accuracy.
- (RCL) a standalone MC code based on Recola 1 [72] amplitudes (version 1.4.4), Collier [73] loop integrals (version 1.2.7), a modified implementation of the Vegas numerical-integration algorithm [74], and the abelianisation of the FKS subtraction scheme for QED IR singularities [75], allowing to compute both diagonal and off-diagonal entries of the decay matrix at NLO EW accuracy.

Excellent agreement was found at integrated and differential level, for the diagonal entries of the decay matrix, providing a strong validation of the results presented in this section.

The numerical results correspond to the following choices for the EW-boson on-shell masses [76],

$$M_{\rm W}^{\rm OS} = 80.377\,\text{GeV}, \qquad M_{\rm Z}^{\rm OS} = 91.1876\,\text{GeV}\,. \tag{3.1}$$

JHEP02(2026)056

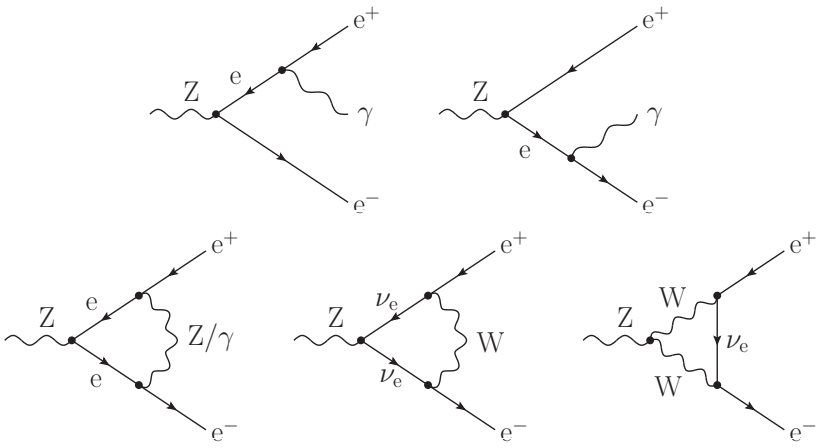

Figure 1. Real (top row) and virtual (bottom row) diagrams contributing to the Z-boson decay into a massless lepton-antilepton pair at NLO EW.

The calculation is performed in the G_μ scheme [77, 78], with the Fermi constant set to $G_\mu = 1.16638 \cdot 10^{-5}\,\text{GeV}^{-2}$. The masses of the top quark and of the Higgs boson are set equal to [76],

$$m_\text{t} = 172.69\,\text{GeV}, \qquad M_\text{H} = 125.25\,\text{GeV}\,. \tag{3.2}$$

The NLO partial decay width for the considered decay (for a single lepton family) features very good agreement between the two independent codes:

$$\Gamma^{(\text{MG5})}_{\ell^+\ell^-} = 0.08383(3)\,\text{GeV}, \qquad \Gamma^{(\text{RCL})}_{\ell^+\ell^-} = 0.083834(4)\,\text{GeV}\,.$$

We have computed all entries of the decay matrix at LO, at exact NLO EW accuracy, and in the EW-virtual approximation [79].[7] In all cases the computation is performed differentially in the polar and azimuthal angle of the positively charged lepton. Since we treat the leptons as massless, in the case of exact NLO EW corrections leptons are clustered together with radiated photons (dressed leptons) if

$$\Delta R_{\ell\gamma} = \sqrt{(y_\ell - y_\gamma)^2 + (\phi_\ell - \phi_\gamma)^2} < R\,, \tag{3.3}$$

with R corresponding to the resolution radius.

In figure 2 we show differential distributions at LO (dashed) and NLO EW (solid) accuracy in the polar and azimuthal decay angle of the dressed lepton ℓ^+, obtained with our direct computation of the Γ^{NLO} entries via HA. The angle is in the Z-boson rest frame and we find that results obtained for $R = 0.01, 0.1, 1$ agree with each other within integration uncertainties. We therefore show only results for the choice $R = 0.1$.

In the left panel the polar decay angle is considered, for the three diagonal entries: left-left $(-1,-1)$, longitudinal-longitudinal $(0,0)$, and right-right $(+1,+1)$. At LO, the three diagonal entries have a quadratic and linear dependence on the cosine of the polar angle, as can be

[7] In this approximation one-loop corrections are included after being IR regulated through the EW generalisation of the Catani operator [80], while hard-real photon contributions are discarded.

JHEP02(2026)056

evinced from eq. (2.5). For the two entries $\Gamma_{\pm1,\pm1}$, corresponding to the transverse helicity of the Z boson, the quadratic dependence on $\cos\theta_{\ell^+}$ is the same at LO and at NLO, as can be understood by the ratio between NLO EW and LO predictions shown in the inset. Instead, the linear term, proportional to η_ℓ, changes sizeably between LO and NLO EW. Performing a quadratic fit of the curves we obtain the values

$$\eta_\ell^{\rm LO} = 0.2131(1)\,, \qquad \eta_\ell^{\rm EW,virt} = 0.1409(1)\,, \qquad \eta_\ell^{\rm NLO} = 0.1405(8)\,, \tag{3.4}$$

where the number in parentheses is the error on the last digit.

We have checked numerically that the analytic form of the decay matrix at NLO EW can be assumed to be equal to the one at the LO.[8] Only the value η_ℓ is modified, receiving corrections of order -35%. Such corrections are almost entirely of virtual origin, since the result does not depend on R and is consistent with the one obtained in the approximation[9] where the real photon emissions are neglected. This outcome, which was not evident a priori and required explicit verification, shows that our numerical evaluation of $\eta_\ell^{\rm NLO}$ agrees very well with the value of $\eta_\ell^{\rm eff}$ (see eq. (2.20)) that has been calculated in ref. [26] with the publicly available Griffin package [81]. Strikingly, the three-body contributions from real-photon radiation have almost no effects in modifying the leading two-body structure of the decay for a Z boson at rest. We will see later in the section that the presence of cuts can change considerably this statement.

The only deviation, which is tiny, from the analytic form that is present at LO is found at the endpoints of the polar-angle distribution for the longitudinal entry $\Gamma_{0,0}$, where a 3% enhancement is found, mostly coming from real-photon corrections and with a mild dependence on the dressing radius (values between $R = 0.01$ and $R = 1.5$ give rather similar results to the angular dependence of $\Gamma_{0,0}$). However, owing to the LO suppression at $\cos\theta = \pm1$, a quadratic fit of the $\Gamma_{0,0}^{\rm NLO}$ distribution gives a result compatible with the LO one within numerical and fit uncertainties. Still, these tiny deviations are a signal of contributions that depend on a higher power of $\cos\theta$, but that numerically have no impact and can be neglected.

In the right panel of figure 2 the azimuthal angle distribution is considered for the real part of the left-longitudinal and left-right entries of the decay matrix, i.e., $\Gamma_{-1,0}$ and $\Gamma_{-1,+1}$. As expected from eq. (2.5), a modulation in $\cos 2\phi_{\ell^+}$ and $\cos\phi_{\ell^+}$ is present for the two terms respectively, and this holds for the NLO results as well. The only difference between LO and NLO is the different amplitude of the $\cos\phi_{\ell^+}$ modulation in the $\Gamma_{-1,0}$ term. In this case, the ratio between NLO and LO results is flat and corresponds to the $\eta_\ell^{\rm NLO}/\eta_\ell^{\rm LO} \simeq 0.66$. Indeed, $\Gamma_{-1,+1}$ does not depend on η_ℓ, while, after integration over θ, $\Gamma_{-1,0} \propto \eta_\ell$. On top of probing the analytic structure of the off-diagonal entries of the decay matrix, this represents a consistency check of our extraction of η_ℓ at NLO. Although it is not shown in figure 2, we have checked that the NLO EW corrections do not change the analytic dependence on $\cos\theta_{\ell^+}$ and ϕ_{ℓ^+} of the imaginary parts of the off-diagonal entries of the decay matrix.

With this calculation, we have excluded further modifications at NLO accuracy to the Z-boson decay matrix, apart from the strikingly large corrections to the value of η_ℓ. However,

[8] Besides performing a fit, we have projected directly on the spherical harmonics the results obtained and verified that, within numerical errors, the structure is the one shown in eq. (2.8).

[9] See footnote 7 for more details.

JHEP02(2026)056

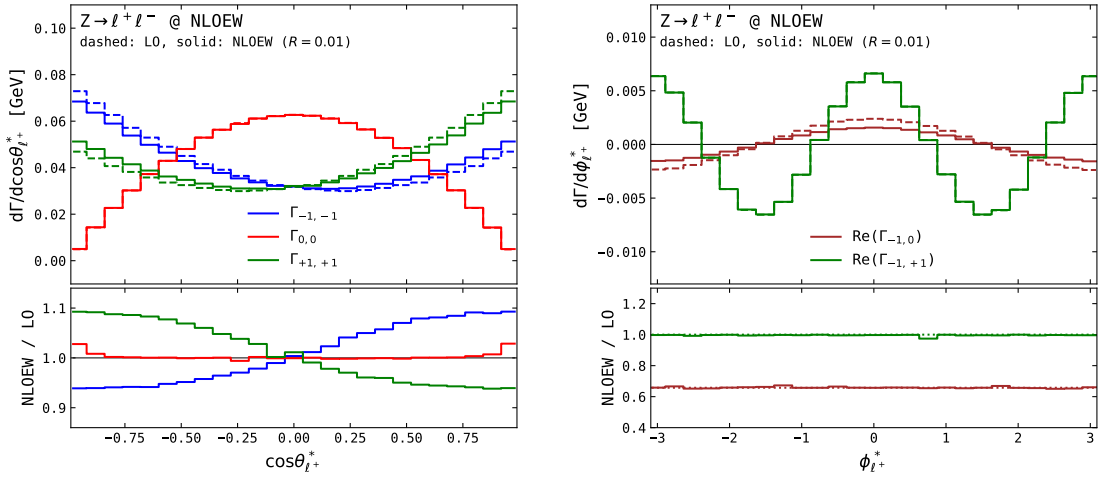

Figure 2. Z-boson decay into a massless lepton-antilepton pair, obtained at LO and NLO EW in the G_μ EW scheme and for $R = 0.01$ dressing resolution. Left figure: diagonal entries of the decay matrix Γ, differentially in the polar decay angle. Right figure: real part of two off-diagonal entries, differentially in the azimuthal decay angle. All results have been obtained through a dummy MC code based on RECOLA 1, version 1.4.4 [72], a modified implementation of the VEGAS numerical-integration algorithm [74], and the FKS subtraction scheme for QED IR singularities [75].

in realistic computations, including also a production mechanism for the Z boson, additional complications arise.

First, while in the calculation for an on-shell Z-boson decay relies on the on-shell masses, in a full-fledged calculation including the production and the decay of EW bosons, the input masses must be the pole ones, converted from the values in eq. (3.1) through the relations of ref. [82]. This holds for calculations performed either in the PA [78, 83, 84] or in the NWA [59, 85], in order to correctly capture partial off-shell effects associated to the intermediate s-channel bosons. The NLO values in eq. (3.4) computed with EW-boson pole masses rather than with on-shell masses are very similar. We found that differences in the two cases are at the per mille level. Thus, this effect can be safely neglected.

Second, at the experimental level, the reference frame of the Z is defined as the one given by the momenta of the $\ell^+\ell^-$ pair. In an NLO EW calculation, for the Born, virtual and real emission contributions with photons clustered to leptons, the $\ell^+\ell^-$ pair and Z rest frames are the same. Instead, for the real emission contributions with non-clustered photons, the two frames are different. We have verified that the angular distributions and the value of η_ℓ^{NLO} extracted in the two frames are equivalent and do not depend on R. However, in the experimental analyses $\ell^+\ell^-$ pairs are also required to have an invariant mass close to M_{Z}^{OS}, in order to be identified as a Z boson.

In figure 3 we focus on the case of $\Gamma_{-1,-1}$ and we show the polar-angle distribution ($\cos\theta$) at LO together with the NLO EW prediction with the cut $M_{\ell^+\ell^-} > 81\,\text{GeV}$ (red) and no cuts (blue), for three different R choices: $R = 1$ (solid), $R = 0.1$ (dashed) and $R = 0.01$ (dotted). Unlike the case with no cuts, there is a dependence on R and, especially, the extracted value for η_ℓ^{NLO} is different. The results are listed for the three cases in table 1. Although the values without the $M_{\ell^+\ell^-}$ cut are perfectly compatible with those of eq. (3.4),

JHEP02(2026)056

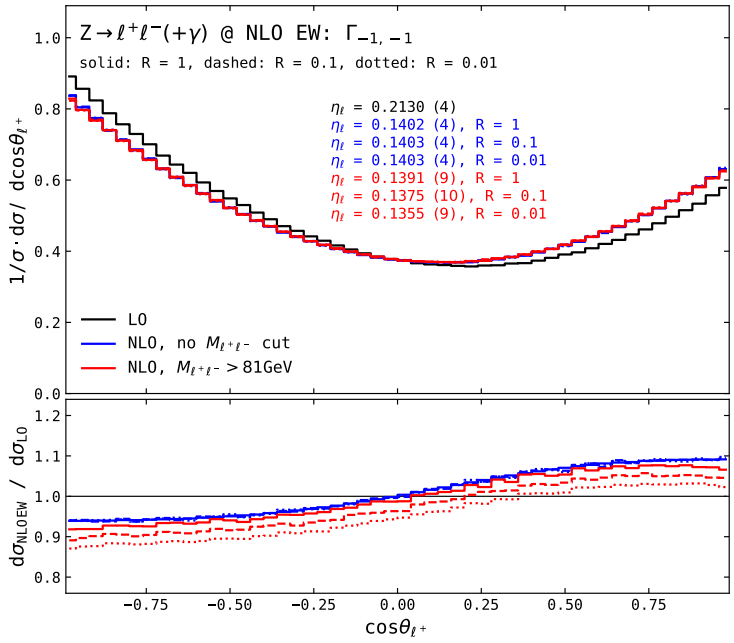

Figure 3. Z-boson decay into a massless lepton-antilepton pair, obtained at LO and NLO EW in the G_μ EW scheme and for various dressing-resolution radii. The entry $\Gamma_{-1,-1}$ of the decay matrix is considered differentially in the polar decay angle. All results have been obtained with a private version of MG5_aMC@NLO [70, 71] that enables the calculation of diagonal entries of the decay matrix at NLO accuracy.

$\eta_\ell^{\rm NLO}$	$R = 1$	$R = 0.1$	$R = 0.01$
$M_{\ell^+\ell^-} > 81\,\text{GeV}$	0.1391(9)	0.1375(10)	0.1355(9)
no $M_{\ell^+\ell^-}$ cut	0.1402(4)	0.1403(4)	0.1403(4)

Table 1. Z-boson spin-analysing power extracted from the polar-angle distribution of the $\Gamma_{-1,-1}$ entry of the decay matrix for three values of the lepton-dressing resolution radius. The invariant mass of the dressed-lepton pair is either uncut or constrained to be larger than 81 GeV.

the differences between the values obtained for $M_{\ell^+\ell^-} > 81\,\text{GeV}$ and those of eq. (3.4) are manifest. They consist of effects of order (at most) 5%, which are definitely much smaller than relative difference between $\eta_\ell^{\rm NLO}$ and $\eta_\ell^{\rm LO}$, but they are not negligible. Furthermore, at the LHC a Z boson is very rarely produced at rest (in the laboratory frame). Since in a realistic set-up the recombination is defined in the laboratory frame, the effective value R in the Z boson rest frame depends on the momenta of the Z boson itself. This aspect is investigated in the next section.

3.2 Z-boson decay in association to the production

The analysis of section 3.1 assumes a Z boson at rest, while in a LHC production processes a Z boson is produced with a non-vanishing transverse momentum, at a given rapidity, and

JHEP02(2026)056

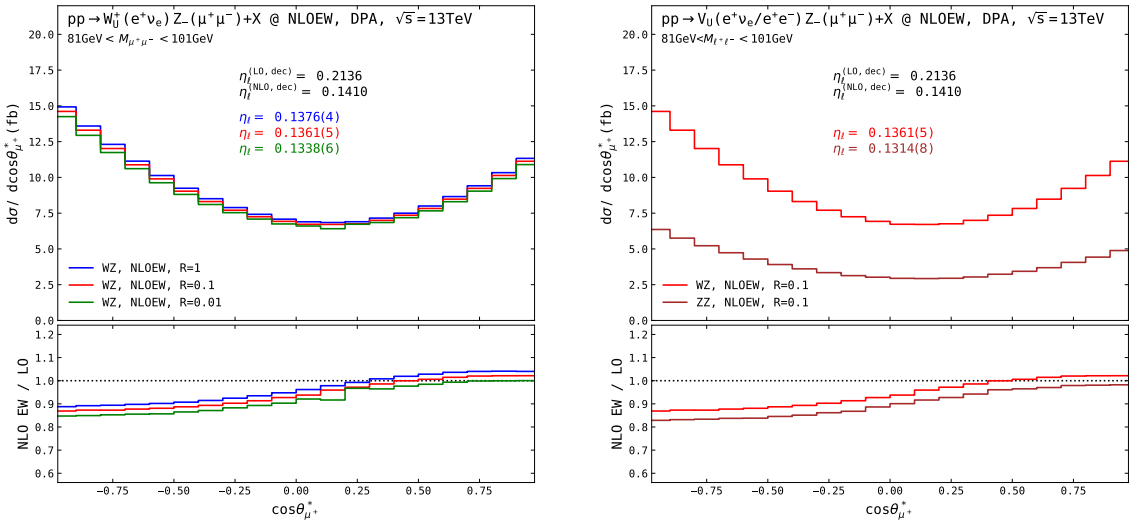

Figure 4. Dependence of polar-angle distributions on the lepton-dressing radius (left) and on the production mechanism (right) for a left-handed Z boson. Left figure: left-handed Z boson produced in association with an unpolarised W boson, using different resolution radii in the lepton-dressing algorithm. Right figure: left-handed Z produced with an unpolarised Z boson (brown) or with an unpolarised W boson (red). An invariant-mass constraint $81\,\text{GeV} < M_{\ell^+\ell^-} < 101\,\text{GeV}$ is applied to opposite-sign same-flavour lepton pairs, and an LHC collision energy of 13 TeV is understood. All results have been obtained with the MoCaNLO code [17, 47, 63].

in association with other particles. In order to study the impact of this different kinematic configuration on the extraction of the spin-analysing power, we consider two specific processes, namely, the inclusive production of a Z boson in association with either another Z boson or a W boson at the LHC, with 13 TeV of centre-of-mass energy:

$$\mathrm{pp} \to \mathrm{Z}(\to \mathrm{e}^+\mathrm{e}^-)\,\mathrm{Z}(\to \mu^+\mu^-), \qquad \mathrm{pp} \to \mathrm{W}^+(\to \mathrm{e}^+\nu_\mathrm{e})\,\mathrm{Z}(\to \mu^+\mu^-)\,. \tag{3.5}$$

We perform the calculation at NLO EW in the DPA with the MoCaNLO general-purpose MC code [17, 47, 63], which is interfaced with Recola 1, version 1.4.4 [72], and relies on the dipole subtraction scheme for QED IR singularities [80, 86, 87].

We stress that the interplay between the dressing algorithm and the decay angles is not trivial, as at the LHC the dressing of charged leptons is applied to momenta evaluated in the laboratory frame, while the angular observables are constructed in the rest frame of target EW bosons, with respect to a certain axis of quantisation of the boson spins. For inclusive ZZ and ZW production it is rather natural [17, 37] to define this axis as the single-boson spatial direction in the boson-pair centre-of-mass frame.

In the left plot of figure 4 we show the distributions in the polar decay angle associated to a left-handed Z boson that is produced together with an unpolarised W^+ boson and that is decaying into leptons. This is equivalent to selecting in eq. (2.10) only the $\lambda = -1$, such that in this case eq. (2.1) can be simplified as

$$\frac{4\pi}{3}\frac{1}{\sigma^{(\mathrm{N})\mathrm{LO}}}\frac{\mathrm{d}^2\sigma^{(\mathrm{N})\mathrm{LO}}}{\mathrm{d}\cos\theta\,\mathrm{d}\phi} = \Gamma^{(\mathrm{N})\mathrm{LO}}_{-1,-1}\,, \tag{3.6}$$

JHEP02(2026)056

$\eta_\ell^{\rm NLO}$	$R = 1$	$R = 0.1$	$R = 0.01$
Z_W$^+$	0.1376(4)	0.1361(5)	0.1338(6)

Table 2. Spin-analysing power $\eta_\ell^{\rm NLO}$ extracted from polar-angle distributions for a left-handed Z produced in association with an unpolarised W$^+$ boson at the LHC (left side of figure 4). Three values of the lepton-dressing radius are considered. An invariant-mass constraint $81\,\text{GeV} < M_{\mu^+\mu^-} < 101\,\text{GeV}$ and a collision energy of 13TeV are understood.

where we have stressed that the relation is valid both at LO and NLO accuracy. Since the $\lambda = -1$ polarisation is chosen, the spin-density matrix is calculated directly on the only spin-state available so the ρ has only one entry and therefore by definition it is equal to one.

We repeat in the following the analysis of section 3.1. In this case we require

$$81\ \text{GeV} < M_{\mu^+\mu^-} < 101\ \text{GeV}\,, \tag{3.7}$$

and apply the standard cone dressing algorithm as applied in ATLAS and CMS spin-correlation and polarisation analyses [37, 64, 66–69], consistently to what has been done in section 3.1.

Both at the inclusive and differential level NLO EW corrections depend on the recombination-radius R, as can be seen in the left plot of figure 4. Thus, also the extracted value for $\eta_\ell^{\rm NLO}$ depends on it, and it is listed in table 2 for the three different choices of R. Similarly to the case of the decay alone, table 1, with a large value of R the extracted value of $\eta_\ell^{\rm NLO}$ gets closer to the value found without cuts, in eq. (3.4), and therefore to $\eta_\ell^{\rm eff}$. With a smaller value of R, more photons escape clustering with charged leptons, leading to a slightly larger deviation from the LO picture. Still, the results in table 2 are different from those in the first row of table 1. Indeed, as expected, the extraction of the spin-analysing power at NLO EW depends on R but also on the kinematics of the Z boson; if the clustering is performed in the laboratory frame, R is not Lorentz-invariant. If a Z boson is produced with a small boost at the LHC, the extracted $\eta_\ell^{\rm NLO}$ will be rather close to the value evaluated as in section 3.1 with the same value of R. On the contrary, in a very boosted kinematic configuration the clustering of photon radiation with charged leptons will be different. This makes the extraction of $\eta_\ell^{\rm NLO}$ inherently process dependent.

In the right panel of figure 4 we consider the polar decay angle associated to a left-handed Z boson decaying into leptons produced either with an unpolarised W$^+$ boson (red curve, same as in the left plot) or with an unpolarised Z boson (brown). The same photon clustering (cone dressing, with $R = 0.1$) is used for the two cases. Besides the different absolute size of the NLO EW corrections in the two processes, the quadratic fit of the distributions gives rather different predictions for $\eta_\ell^{\rm NLO}$, shown in table 3. The Z boson is slightly more boosted in ZZ production ($p_{\rm T}(\text{Z}) \approx 40\,\text{GeV}$) than in ZW ($p_{\rm T}(\text{Z}) \approx 25\,\text{GeV}$), which explains why the η_ℓ value extracted in the ZW case (0.136) is closer to the value for a Z at rest w.r.t. the one obtained for ZZ (0.132). Another aspect which is worth recalling is that individual helicity states are defined in a specific Lorentz frame [17], therefore the evaluation of the spin-analysing power at NLO EW mildly depends on the chosen coordinate system: a left-handed Z boson with the helicity quantised in the laboratory frame and a left-handed Z boson with the

JHEP02(2026)056

$\eta_\ell^{\rm NLO}$	Z_W$^+$	Z_Z
$R = 0.1$	0.1362(8)	0.1326(7)

Table 3. Spin-analysing power $\eta_\ell^{\rm NLO}$ extracted from polar-angle distributions for a left-handed Z produced in association with an unpolarised W$^+$ or Z boson at the LHC (right side of figure 4). An invariant-mass constraint 81 GeV $< M_{\ell^+\ell^-} <$ 101 GeV and a collision energy of 13 TeV are understood.

helicity quantised in another Lorentz frame are produced with different kinematics, so, strictly speaking, the two of them come from different production mechanisms.

The overall result of this section is that the correct evaluation of the spin-analysing power η_ℓ in the presence of higher-order EW corrections has to be carried out case by case. In other words, the presence of real-photon radiation leads to a dependence on the resolution radius of the dressing algorithm and on the mechanism producing the Z boson when a cut as the one in eq. (3.7) is present. Furthermore, although we have presented results on the dependence on the resolution radius using a standard cone dressing algorithm, we have checked that changing the clustering procedure, e.g. the generalised k_t one [88], leads to small changes in the evaluation of $\eta_\ell^{\rm NLO}$. That said, we understand that evaluating the corrected η_ℓ depending on the process and the boost of the Z boson in unpractical in an analysis on real data that may impose various phase-space selections. Nevertheless, it is important to estimate such effects and consider them as a source of systematic uncertainty.

4 Inclusive Z-boson pair production at the LHC

We can now compare the results obtained via QT and the HA method. We start considering the inclusive production of ZZ pairs at 13 TeV, with one Z boson decaying into muons and the other into an electron-positron pair, as in eq. (3.5). We have performed all calculations that are discussed in this section with the help of the MoCaNLO code [17, 47, 63], employing the same input parameters of section 3.1. The MoCaNLO code enables the direct computation of the spin-density-matrix entries by selecting specific helicity states for intermediate bosons in Born, real and virtual amplitudes, owing to a flexible interface to the Recola 1 library [72]. Also, via this code it is possible to perform the calculation either taking into account full off-shell effects or in DPA. Thus, QT can be applied in both cases and validated against the HA method in DPA.

We focus on the coefficient γ_{1010}, which is related to the left- and right-helicity content of the diboson process [17]. Via the HA method it can be written as

$$\gamma_{1010} = -\frac{3\,{\eta_\ell}^2}{16\pi}\,(f_{--} + f_{++} - f_{-+} - f_{+-}) = {\eta_\ell}^2 F_\pm\,, \tag{4.1}$$

with

$$f_{ab} \equiv \rho_{aabb}\,, \quad \text{and} \quad F_\pm \equiv -\frac{3}{16\pi}\,(f_{--} + f_{++} - f_{-+} - f_{+-})\,. \tag{4.2}$$

As it is manifest, f_{ab} corresponds to the diagonal entry ρ_{aabb} of the spin-density matrix, namely the joint helicity fraction for two intermediate Z bosons with helicities a and b, respectively.

JHEP02(2026)056

We consider massless leptons and apply to both the same-flavour lepton pairs the invariant-mass constraint

$$81\,\text{GeV} < M_{\ell^+\ell^-} < 101\,\text{GeV}\,, \qquad \ell = \text{e}, \mu\,, \tag{4.3}$$

as in eq. (3.7). Note that in the generic case of two different-flavour lepton-antilepton pairs the factor η_ℓ^2 is replaced by the product $\eta_\ell^{(1)} \cdot \eta_\ell^{(2)}$, where the two spin-analysing powers take slightly different values owing to possibly different cuts applied to the two Z-boson virtualities. The same consideration would hold if the two fermion-antifermion pairs are characterised by different $\text{SU}(2)_L$ and $\text{U}(1)_Y$ quantum numbers, e.g. in the decay channel with two leptons and two quarks.

The direct calculation at LO and at NLO EW, via the HA method, of the spin-analysing power η_ℓ and of the quantity $F_\pm$ (defined in eq. (4.1)) returns,

$$F_\pm^{\text{LO}} = -0.0389(1), \quad F_\pm^{\text{NLO}} = -0.0388(1), \qquad \eta_\ell^{\text{LO}} = 0.2136(3), \quad \eta_\ell^{\text{NLO}} = 0.1313(7)\,. \tag{4.4}$$

Using the same convention adopted in the previous sections for denoting results at LO, NLO EW accuracy and their difference, at NLO EW we obtain

$$\begin{aligned}(\eta_\ell^{\text{NLO}})^2(F_\pm^{\text{NLO}}) &= (\eta_\ell^{\text{LO}} + \delta\eta_\ell^{\text{NLO}})^2(F_\pm^{\text{LO}} + \delta F_\pm^{\text{NLO}}) \\ &= (\eta_\ell^{\text{LO}})^2(F_\pm^{\text{LO}}) + 2\,\eta_\ell^{\text{LO}} \cdot \delta\eta_\ell^{\text{NLO}} \cdot F_\pm^{\text{LO}} + (\eta_\ell^{\text{LO}})^2 \cdot \delta F_\pm^{\text{NLO}} + \mathcal{O}(\alpha_{\text{ew}}^2) \\ &= \gamma_{1010}^{\text{NLO}} + \mathcal{O}(\alpha_{\text{ew}}^2)\,.\end{aligned} \tag{4.5}$$

Thus we can write

$$\gamma_{1010}^{\text{LO}} = (\eta_\ell^{\text{LO}})^2(F_\pm^{\text{LO}})\,, \qquad \gamma_{1010}^{\text{NLO}} = \gamma_{1010}^{\text{LO}} + 2\,\eta_\ell^{\text{LO}} \cdot \delta\eta_\ell^{\text{NLO}} \cdot F_\pm^{\text{LO}} + (\eta_\ell^{\text{LO}})^2 \cdot \delta F_\pm^{\text{NLO}}\,, \tag{4.6}$$

which lead to the following predictions,

$$\text{HA (DPA)}: \qquad \gamma_{1010}^{\text{LO}} = 0.001775(1), \qquad \gamma_{1010}^{\text{NLO}} = 0.000407(3)\,. \tag{4.7}$$

Applying the QT approach directly on the four-lepton momenta, using the calculation in the DPA, we obtain

$$\text{QT (DPA)}: \qquad \gamma_{1010}^{\text{LO}} = 0.001774(5), \quad \gamma_{1010}^{\text{NLO}} = 0.000404(6)\,. \tag{4.8}$$

The values in eq. (4.7) and eq. (4.8) are in perfect agreement, validating our procedure.

We have also checked that taking into account the full off-shell corrections, including non-resonant effects, and performing the QT,

$$\text{QT (full)}: \qquad \gamma_{1010}^{\text{LO}} = 0.001708(2), \quad \gamma_{1010}^{\text{NLO}} = 0.000411(9)\,. \tag{4.9}$$

the differences with eq. (4.8) are very mild.[10]

These results further confirm that the largest effects for the coefficients $\gamma_{1m1m'}$ originate from the NLO corrections to the spin-analysing power η_ℓ, while minor effects are found for

[10] We reckon that the good agreement also between the QT (full) and HA (DPA) results is favoured by the presence of the cuts in eq. (4.3), which select the *on-shell* region.

JHEP02(2026)056

the spin-density matrix at the production-level. It is manifest from eq. (4.4) that the quantity $\delta F_{\pm}^{\rm NLO}$ is completely negligible. Also, by comparing eqs. (2.19) and (4.6), it is clear that the quantity $F_{\pm}$ and C_{1010} are the same quantity with a different normalisation

$$C_{1010} = 8\pi F_{\pm}\,, \tag{4.10}$$

so also NLO EW corrections to C_{1010} are negligible: $C_{1010}^{\rm NLO} \simeq C_{1010}^{\rm LO}$.

We can now proceed in the opposite direction and test whether starting from the calculation of γ_{1010} with the QT at NLO EW, it is possible to match the analytical NLO EW prediction for C_{1010} (or, alternatively, $F_{\pm}$). We perform this test using only the DPA results. First of all, we take as a benchmark the value computed via the HA method,

$$C_{1010}^{\rm NLO} \simeq C_{1010}^{\rm LO} = \frac{8\pi\gamma_{1010}^{\rm LO}}{(\eta_\ell^{\rm LO})^2} = 0.977\,. \tag{4.11}$$

The above formula is the one used in the LO QT procedure to reconstruct the aforementioned C coefficient. Then, we write different definitions of C_{1010}, adopting different choices in the extraction from $\gamma_{1010}^{\rm NLO}$: *(1)* dividing by the LO value of the spin-analysing power $(\eta_\ell^{\rm LO})^2$, *(2)* dividing by the NLO value $(\eta_\ell^{\rm NLO})^2$ or *(3)* taking into account the expansion $(\eta_\ell^{\rm NLO})^2 + 2\,\eta_\ell^{\rm LO}\cdot\delta\eta_\ell^{\rm NLO}$. Also, for the last two choices, we look at the difference between *(a)* using $\eta_\ell^{\rm NLO}$ for the process and cuts considered, and the specific recombination-radius R that has been chosen and *(b)* the value at the simple decay level without cuts, which corresponds to $\eta_\ell^{\rm eff}$ in eq. (2.20):

$$\frac{8\pi\gamma_{1010}^{\rm NLO}}{(\eta_\ell^{\rm LO})^2} = 0.224 \qquad \textit{(1)} \tag{4.12}$$

$$\frac{8\pi\gamma_{1010}^{\rm NLO}}{(\eta_\ell^{\rm NLO})^2} = 0.593 \qquad \textit{(2a)} \tag{4.13}$$

$$\frac{8\pi\gamma_{1010}^{\rm NLO}}{(\eta_\ell^{\rm eff})^2} = 0.518 \qquad \textit{(2b)} \tag{4.14}$$

$$\frac{8\pi\gamma_{1010}^{\rm NLO}}{(\eta_\ell^{\rm LO})^2 + 2\,\eta_\ell^{\rm LO}\cdot\delta\eta_\ell^{\rm NLO}} = 0.977 \qquad \textit{(3a)} \tag{4.15}$$

$$\frac{8\pi\gamma_{1010}^{\rm NLO}}{(\eta_\ell^{\rm LO})^2 + 2\,\eta_\ell^{\rm LO}\cdot\delta\eta_\ell^{\rm eff}} = 0.710 \qquad \textit{(3b)} \tag{4.16}$$

The result in eq. (4.12) is the standard QT procedure applied to a NLO EW calculation, where using a LO value for the spin-analysing power the NLO EW corrections to this quantity are erroneously propagated to the spin-density matrix ρ. The result in eq. (4.14) is the procedure proposed in ref. [26]. It is interesting to note that only the procedure in eq. (4.15) returns the correct NLO value of C_{1010}, which we have computed via the HA method and turns out to be equal to the LO value up to per mille effects.

We want to stress that the conclusion of this check is *not* that the procedure used in eq. (4.15) is the correct one to be applied to data when performing QT. Indeed, data is not at NLO EW accuracy, as it naturally takes into account higher-order effects. This test is precisely saying that the higher-order effects induced by the combined one-loop corrections to both Z decays, which effectively consist of two-loop corrections from NNLO EW corrections,

JHEP02(2026)056

are *not* negligible. The difference between eqs. (4.13) and (4.15) or eqs. (4.14) and (4.16) are those $\mathcal{O}(\alpha_{\rm ew}^2)$ effects that have been discarded in the second line of eq. (4.5). In fact, when QT is applied to data, one should use the definition in eqs. (4.13), where $\eta_\ell^{\rm NLO}$ has been calculated for the specific process and cuts considered. The usage of $(\eta_\ell^{\rm eff})^2$ is definitely an improvement w.r.t. $(\eta_\ell^{\rm LO})^2$, but non optimal. Moreover, as already mentioned before, if different cuts are present for the two Z bosons, the quantity $\eta_\mu^{\rm NLO}\eta_e^{\rm NLO}$ should be used in the normalisation, with $\eta_\ell^{\rm NLO}$ calculated for the $\mu^+\mu^-(e^+e^-)$ pair when $\ell = \mu(e)$.

In the next section we further support the statements of the previous paragraph considering a simplified scenario and we discuss the limitations for the case of the SM Higgs decaying into four leptons.

5 Z-boson pairs from a (heavy) Higgs-boson decay

In this section, we consider a system whose spin structure is much more constrained — and therefore simpler — than that of inclusive ZZ production at the LHC: the decay of a scalar particle into a pair of Z bosons. Our primary interest is the case where the scalar corresponds to the SM Higgs boson, but we will focus the discussion on the academic scenario in which $M_{\rm H} > 2M_{\rm Z}$, as in the case of possible other scalar particles that are present in new-physics extensions of the SM. The purpose of this study is twofold.

First, in section 5.1, we aim to show that in the case of a heavy Higgs boson with $M_{\rm H} \gg 2M_{\rm Z}$ the procedure outlined in the previous section can be applied to extract the correct spin-density matrix at NLO EW accuracy, since both Z bosons in the $\rm H \to ZZ$ decay are predominantly on-shell. On the contrary, decreasing the value of $M_{\rm H}$, off-shell contributions become more and more relevant, reducing the reliability of this approach and rendering it entirely invalid for $M_{\rm H} \leq 2M_{\rm Z}$, as in the SM.

Second, for the regime $M_{\rm H} \gg 2M_{\rm Z}$, where both Z bosons are mostly on-shell as in ZZ production, we perform an approximate NNLO EW calculation by taking into account NLO EW effects in both decays. This test, which is presented in section 5.2, provides an explicit example that supports the strategy proposed at the end of the previous section for extracting the correct spin-density matrix from data.

In all these sections the calculations for the HA method are performed in NWA,[11] and in general, both for QT and HA results, we use the same input parameters employed in the previous sections.

Since the interplay between selection cuts and lepton-photon recombination has been broadly discussed in section 3.2, the results of this section have been obtained in a simplified setup in that regards. The HA results at NLO properly include (factorisable) virtual and real-photon corrections in the NWA, but the lepton dressing is applied to momenta written in the single-Z-boson rest frame. In spite of this simplification, the NLO EW accuracy is not spoiled. Furthermore, up to a technical cut ($M_{\ell^+\ell^-} > 10\,\text{GeV}$), we are inclusive on the lepton-pair invariant masses, in order to avoid sensitivity to the details of the dressing algorithm.

[11] For technical limitations the MoCaNLO MC framework cannot deal with Higgs-boson decays in the DPA, therefore a simple standalone code based on Recola 1.4.4 [72] has been devised for the $\rm H \to ZZ \to 4\ell$ decay process in the NWA at LO and NLO EW accuracy.

JHEP02(2026)056

5.1 Off-shell effects in H → ZZ

If we consider a heavy Higgs boson that shares all the properties of the SM Higgs except for its mass, and examine the decay $H \to \mathrm{ZZ}$, most of the entries of the spin-density matrix of the ZZ system vanish. Thus, at variance with generic boson-pair production, the relevant quantum-information observables only depend on few independent α, γ coefficients. As an example, in the case of the heavy Higgs decay eqs. (4.1) and (4.10) combined together reads

$$C_{1010} = 8\pi F_{\pm} = -3\, f_{--}\,. \tag{5.1}$$

Indeed, the structure of the SM scalar-to-gauge coupling leads to the relations $f_{\pm\mp} = 0$ and $f_{++} = f_{--}$. The analogous relation for C_{111-1} is instead

$$C_{111-1} = -3\ \mathrm{Re}\,(\rho_{-\mathrm{L}-\mathrm{L}})\,. \tag{5.2}$$

In the following we consider four representative values for the Higgs-boson mass,

$$M_{\mathrm{H}} = (183,\ 200,\ 225,\ 250)\ \mathrm{GeV}\,. \tag{5.3}$$

The condition $M_{\mathrm{H}} > 2M_{\mathrm{Z}}$ is valid for all of them, opening up the possibility to produce two on-shell Z bosons. QT results at LO and NLO EW accuracy have been obtained with the help of MadGraph5_aMC@NLO [70, 71] simulating the full process

$$\mathrm{H} \to \mathrm{e}^+\mathrm{e}^-\mu^+\mu^-\,, \tag{5.4}$$

using the recombination radius $R = 1.0$,[12] and requiring $M_{\ell^+\ell^-} > 10$ GeV for both same-flavour lepton pairs. Such an inclusive cut on the lepton-pair invariant masses has been chosen with the purpose of being as close as possible to the HA results obtained in the NWA,

$$\mathrm{H} \to \mathrm{Z}(\to \mathrm{e}^+\mathrm{e}^-)\,\mathrm{Z}(\to \mu^+\mu^-)\,. \tag{5.5}$$

While in the case of inclusive ZZ production at the LHC the centre-of-mass coordinate system of the four dressed leptons (which we dub "CM") is the most natural choice for the spin quantisation, in the case of the Higgs decay the Higgs rest frame (which we dub "HR") is often used [23, 26]. The two frames are equivalent at LO, but are different at NLO due to (the small fraction of) unclustered photon radiation. We have checked numerically that the two frame choices give very similar results at NLO for the observables investigated here. This is in agreement with previous literature results [17, 26]. Therefore, we present only the results in the HR frame. Following the same procedure discussed in section 4, in particular eqs. (4.5) and (4.6), we derive the predictions via the HA methods for γ_{1010} at LO and NLO accuracy, using for η_ℓ^{LO} the usual value in eq. (2.6), and for the other inputs the values in table 4. As can be noticed, the value of η_ℓ^{NLO} depends on the value of M_{H}, which enters via loop corrections. Both the helicity fractions and η_ℓ^{NLO} are computed at exact NLO EW corrections.

The values of γ_{1010} obtained via the HA method for the four benchmark masses in (5.3) are listed in table 5 and compared with the corresponding results obtained via QT. We note from the previous equations that also for this process the values of $F_\pm$, and therefore of also the "true values" of C_{1010}, receive very mild NLO EW corrections.

[12] Nevertheless, we have verified that also with $R = 0.1$ the results would be indistinguishable with our numerical accuracy.

JHEP02(2026)056

M_{H} [GeV]	η_ℓ^{NLO}	f_{--}^{LO}	f_{--}^{NLO}
183	0.1420(4)	0.3303	0.3304
200	0.1423(4)	0.2516	0.2537
225	0.1432(4)	0.1619	0.1644
250	0.1439(4)	0.1041	0.1059

Table 4. Spin-analysing power η_ℓ^{NLO} calculated at NLO EW and helicity fraction f_{--} calculated at LO and NLO EW, for the different M_{H} benchmark points. MC-integration uncertainties are shown in parentheses, if not shown they are smaller than 10^{-4}.

γ_{1010} coefficient ($\times 10^3$)				
	QT		HA	
M_{H}	LO	NLO	LO	NLO
183 GeV	−1.5506(9)	−0.44(1)	−1.790(1)	−0.596(6)
200 GeV	−1.3085(5)	−0.417(9)	−1.364(1)	−0.469(5)
225 GeV	−0.8601(7)	−0.294(7)	−0.8776(7)	−0.315(3)
250 GeV	−0.559(1)	−0.200(3)	−0.5643(4)	−0.208(2)

Table 5. Numerical results for the γ_{1010} coefficient (inflated by a factor 10^3) extracted via QT from full off-shell simulations and via HA methods by direct calculation with intermediate on-shell Z bosons, using eqs. (4.5) and (4.6) and inputs from table 4. The Z bosons are identified by the flavour of the decay products and the spin-quantisation axis is given by the direction of the Z decaying to the e^+e^- pair in the Higgs reference frame (HR). MC-integration uncertainties are shown in parentheses.

The γ_{1010} coefficient is generally small, as in ZZ production, and decreases for large Higgs-boson masses. Indeed, at large M_{H} the longitudinal polarisations of the two Z bosons is favoured, both at LO and NLO EW. Since f_{LL} increases, f_{--} must decrease.

For masses above $M_{\mathrm{H}} = 225\,\mathrm{GeV}$, although Z off-shell effects are taken into account only in the QT result, the HA method, which is performed in NWA, reproduces very well both the LO and NLO predictions. While a fairly good agreement is found also for the intermediate cases, the Higgs mass $M_{\mathrm{H}} = 183\,\mathrm{GeV} \gtrsim 2M_{\mathrm{Z}}$ leads to a larger discrepancy. We notice that the discrepancy (QT/HA = 0.87 at LO) is even larger at NLO (QT/HA = 0.77).

When the mass of the Higgs is just above the value $2M_{\mathrm{Z}}$, the two Z bosons emerging from the decay are almost at rest in the Higgs rest frame. Thus, in the absence of invariant-mass constraints forcing the same-flavour, opposite-sign lepton pairs to be close to M_{Z}, a sizeable fraction of off-shell events, which at NLO are simulated including both resonant and non-resonant diagrams, will feature at least one of the two lepton pairs with an invariant mass that is far from the on-shell region. This feature can be easily seen in the left plot of figure 5 where we compare, for $M_{\mathrm{H}} = 183$ GeV, the invariant-mass spectrum at NLO

JHEP02(2026)056

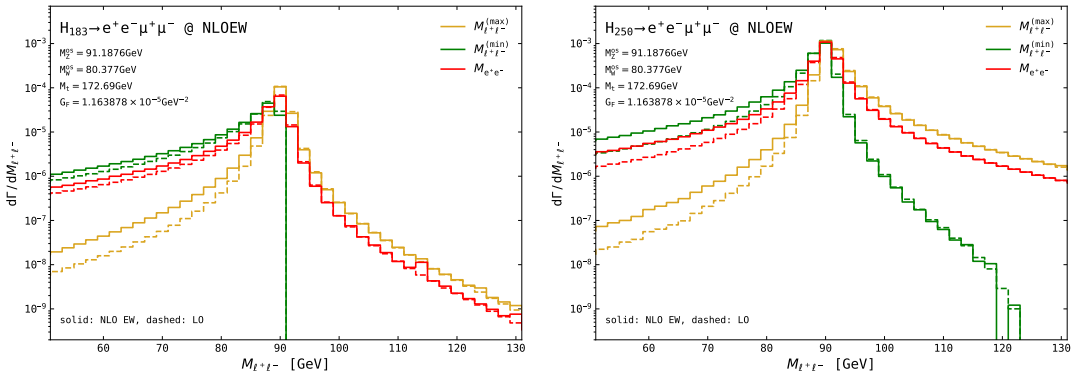

Figure 5. Invariant-mass distributions of the same-flavour lepton pair with the largest/smallest invariant mass (yellow/green) and of the electron-positron pair (red) in the $\mathrm{H} \to e^+e^-\mu^+\mu^-$ off-shell process, for $M_\mathrm{H} = 183\,\mathrm{GeV}$ (left) and $M_\mathrm{H} = 250\,\mathrm{GeV}$ (right). Solid curves: NLO EW, dashed curves: LO. A lepton-dressing resolution radius of $R = 0.1$ is understood at NLO EW.

(solid lines) and LO (dashed lines) for three different lepton-pair definitions. Red lines refer to the lepton pair identified via its specific flavour, which for definiteness we choose as e: $M_{e^+e^-}$. Ochre (Green) lines refer to the same-flavour lepton pair with the largest (smallest) invariant mass: $M^{\max}_{\ell^+\ell^-}$ ($M^{\min}_{\ell^+\ell^-}$).

We notice that the typical Breit-Wigner line-shape is present only for the distribution of $M^{\max}_{\ell^+\ell^-}$. Instead, in the case of $M_{e^+e^-}$ many events are off-shell, with lower values than M_Z, and even more for $M^{\min}_{\ell^+\ell^-}$. In other words, for $M_{e^+e^-}$ and $M_{\mu^+\mu^-}$, which are identical, the off-shell fraction is very large and even larger at NLO w.r.t. the LO case. On the contrary, the off-shell fraction for $M^{\max}_{\ell^+\ell^-}$ is very small, while $M^{\min}_{\ell^+\ell^-}$ is almost always off-shell.

Looking at the right plot of figure 5, we find the same information as in the left one but for $M_\mathrm{H} = 250$ GeV, showing a very different picture. The $M_{e^+e^-}$ distribution features the typical Breit-Wigner lines-shape, while the $M^{\max}_{\ell^+\ell^-}$ ($M^{\min}_{\ell^+\ell^-}$) distribution is tilted towards large (small) invariant-mass values. Thus, a large fraction of events have both $M^{\max}_{\ell^+\ell^-}$ and $M^{\min}_{\ell^+\ell^-}$ pairs that are off-shell. On the contrary, both $M_{e^+e^-}$ and $M_{\mu^+\mu^-}$ are typically on-shell.

The QT results for $M_\mathrm{H} = 183$ GeV, unlike those for high masses, are biased by the presence of non-resonant effects, which therefore affect the two-qutrit interpretation of the angular coefficients. One could significantly mitigate this effect by applying strict cuts around M_Z on the same-flavour lepton pairs, but this condition would not be anyway possible for the case $M_\mathrm{H} = 125$ GeV.[13]

In conclusion, while it is tempting to apply the proposed strategy outlined at the end of section 4 to the decay of a SM Higgs boson to four charged leptons, this is not possible

[13]The coordinate system is defined with the spin-quantisation axis aligned to the Z boson labeled V_1. Since each Z is reconstructed from same-flavor leptons, the only ambiguity is in the assignment of V_1. Here, we follow ref. [17] and assign V_1 according to the flavor of its decay leptons. Alternatively, V_1 can be chosen as the lepton pair with the largest invariant mass [23, 25, 26]. As shown in figure 5, this choice induces an asymmetry between V_1 and V_2 ($\alpha^{(1)}_{lm} \neq \alpha^{(2)}_{lm}$), complicating interpretation without invariant-mass constraints. For $M_\mathrm{H} = 183$ GeV, both definitions have drawbacks: the flavor-based choice yields asymmetric invariant-mass distributions for V_1 and V_2, while the mass-based choice enhances their difference.

JHEP02(2026)056

QT ($M_{\rm H} = 250\,\text{GeV}$)	LO	NLO from eq. (4.12)	NLO from eq. (4.15)
C_{1010}	−0.3094(7)	−0.114(4)	−0.315(7)
C_{111-1}	0.849(1)	0.319(4)	0.92(1)
	LO	NLO	
C_{222-2}	0.3106(2)	0.3130(4)	—
C_{212-1}	−0.8508(1)	−0.8531(3)	—
C_{2020}	1.6895(2)	1.6682(6)	—

Table 6. Spin-correlation coefficients $C_{lml'm'}$ extracted with QT from $\text{H} \to \text{e}^+\text{e}^-\mu^+\mu^-$ events at LO and at NLO EW accuracy. A Higgs-boson with $M_{\rm H} = 250\,\text{GeV}$ is considered. MC-integration uncertainties are shown in parentheses.

owing to the unavoidable large off-shell effects. The SM Higgs mass forbids the presence of two intermediate on-shell bosons and therefore critically affects the spin interpretation of the results extracted through QT [17, 23]. At $M_{\rm H} = 250$ GeV, the approach would work, but already with $M_{\rm H} = 183$ GeV, where both Z bosons can still be in principle on-shell, this strategy starts to degrade. It is therefore natural to expect that this strategy would completely fail for $M_{\rm H} = 125$ GeV. In addition, no sensible way to calculate the "true" C_{1010} value is possible. Nonetheless, the production of two qutrits in a spin-singlet state, i.e. from the decay of a scalar, is very interesting in light of a quantum-information interpretation. Several studies have indeed shown how this final state could be used to study entanglement, Bell non-locality, and multipartite entanglement [6–28]. Given our findings, we further confirm the message of ref. [23]: modifications of the definition of quantum-information observables have to be employed, so that they do not depend on the C_{1m1-m} coefficients.

The correct value of η_ℓ is mandatory for a reliable extraction of C coefficients not only for ZZ production, but whenever the Z bosons are on-shell. We explicitly show it in another case: an hypothetical beyond-the-SM heavy scalar. It is important to keep in mind that besides their relevance in the context of quantum-information, it has been shown the spin-density matrix coefficients can also leverage the sensitivity in the searches for new physics [11–13, 18, 22, 23].

In table 6 we show the C_{1010} and C_{111-1} coefficients extracted from a LO simulation via QT and also from an NLO simulation, either following the same procedure at LO, namely eq. (4.12), or considering the correct value of η_ℓ and taking into account the expansion in powers of $\alpha_{\rm ew}$, namely eq. (4.15). We also show the C_{222-2}, C_{212-1} and C_{2020} coefficients, where the η_ℓ dependence is not present and no ambiguity is present. The large effects (falsely) induced by NLO EW corrections to C_{1010} and C_{111-1}, and that are visible in the second column of numerical values, are not present in the third column, similarly to what is already observed in C_{222-2}, C_{212-1} and C_{2020} coefficients.

Using a proper value of η_ℓ is paramount for a reliable extraction of the C parameters. We stress that the conclusion is *not* that the procedure used in eq. (4.15) is the correct one to be applied on data when performing QT. We further explore this fact in the next section.

JHEP02(2026)056

5.2 Optimal approach for extracting C coefficients from pseudo-data

In section 4 we have shown that performing an NLO EW calculation, the correct value of the $C_{1m1m'}$ coefficients can be extracted via QT only using the NLO EW value of η_ℓ, and the prescription in eq. (4.15). An analogous result has been demonstrated for the case of the Higgs decay with $M_{\rm H} = 250\,\text{GeV}$, in tables 5 and 6. We argued in the discussion around eqs. (4.12)–(4.16) that using the procedure in eq. (4.15) rather than eq. (4.13) is a signal that higher-order effects are important, and that the latter should be used with real data. In the following we further support these statements, considering the case of an Higgs decay with $M_{\rm H} = 250\,\text{GeV}$.

The first step in our argument consists in identifying a procedure in order to take into account higher-order effects and therefore simulate as close as possible, for what concerns higher-order corrections, pseudo-data. From discussions in the previous sections it is clear that while NLO EW corrections to the ρ density matrix are minimal,[14] the NLO EW corrections to the Z-boson decay into leptons, and especially η_ℓ, are anomalously large. Thus, it is important to take into account NLO EW corrections to the decay of both Z bosons in a multiplicative way, i.e., as the r.h.s. of eq. (2.14) but with all quantities at NLO EW accuracy.

In order to achieve the aforementioned accuracy, we have devised a simplified approach that captures the dominant effects. We illustrate it by simulating the $\text{H} \to \text{e}^+\text{e}^-\mu^+\mu^-$ process at LO and for $M_{\rm H} = 250\,\text{GeV}$, using the $\{G_\mu,\, M_{\rm Z},\, \sin^2\theta_{\rm w}^{\rm eff}\}$ input EW scheme [29–36], with G_μ and $M_{\rm Z}$ as in section 3.1 and

$$\sin^2\theta_{\rm w}^{\rm eff} = 0.23192\,. \tag{5.6}$$

Note that the input value of the mixing angle in eq. (5.6) has been chosen equal to the value obtained in the G_μ scheme including one-loop EW corrections (for $M_{\rm H} = 250\,\text{GeV}$) as done in section 3.1. In this way, the simulation effectively takes into account NLO corrections to both decays at the same time, without discarding the $\mathcal{O}(\alpha_{\rm ew}^2)$ terms of eq. (4.5), unlike what has been done so far following eq. (4.6). The QT analysis of the results of this simulation can be compared with a value for the HA method, which can be derived in the G_μ scheme employing directly the l.h.s. of eq. (4.5), without discarding $\mathcal{O}(\alpha_{\rm ew}^2)$ terms.

We dub the aforementioned approximation aNNLO, as "approximate NNLO", and we find the following results:

$$\text{QT}: \qquad \gamma_{1010}^{\rm aNNLO} = -0.000262(6)\,, \tag{5.7}$$

$$\text{HA}: \qquad \gamma_{1010}^{\rm aNNLO} = -\frac{3}{8\pi}\left(\eta_\ell^{\rm NLO}\right)^2 \cdot f_{--}^{\rm NLO} = -0.000262\,. \tag{5.8}$$

We find a very good agreement between the two procedures and therefore we can derive the following statements:

- From table 4 we see that at $M_{\rm H} = 250$ GeV the LO prediction for γ_{1010} receives about -63% corrections at NLO EW. If the comparison is instead done between the LO and aNNLO predictions, corrections amount at -54%, i.e., the approximated aNNLO EW corrections are roughly $+10\%$ of the LO prediction and especially $+26\%$ of the

[14] It can be seen by comparing LO and NLO values in eq. (4.4) for $F_\pm$ and in table 4 for f_{--}.

JHEP02(2026)056

NLO EW prediction. Such effects must be taken into account, not only for the sake of precision.

- Since f_{--} is directly related to C_{1010}, as shown in eq. (5.1), and we see explicitly in eq. (5.8) that it is proportional to $\left(\eta_\ell^{\rm NLO}\right)^2$, in order to extract the correct value of C_{1010} the procedure to follow is the one in eq. (4.13), i.e., precisely dividing by $\left(\eta_\ell^{\rm NLO}\right)^2$. We would obtain the value $C_{1010}^{\rm aNNLO} = -0.309(8)$, which by construction is in agreement with the LO and NLO values in table 6.

Thus, we clearly see that, for processes in which the Z bosons are on-shell and decay into leptons, higher-order EW effects can be sizeable and must be taken into account. The proper extraction of the $C_{1m1m'}$ coefficients must be performed following eq. (4.13), possibly taking into account the effects of cuts on the Z decay products, as discussed in section 3.2.

6 Conclusions and outlook

In this work we have carried out a systematic study of the quantum-tomography (QT) extraction of the Z-boson spin-density matrix at next-to-leading-order (NLO) electroweak (EW) accuracy. Our analysis elucidates the origin of the unexpectedly large NLO effects reported in earlier studies [17, 23, 26] and provides a robust framework for incorporating EW corrections into the determination of spin-correlation observables.

First, we have computed the complete NLO EW corrections to the decay matrix of a single on-shell $\mathrm{Z} \to \ell^+\ell^-$ transition. We have shown that the analytic structure of the matrix remains unaltered with respect to the leading-order (LO) expression, while the spin-analysing power η_ℓ receives a sizeable negative shift of approximately -35%. This effect, mostly coming from loop corrections, accounts for the dominant NLO impact observed in previous QT-based analyses.

Second, we have investigated the implications of photon radiation and lepton-dressing algorithms, particularly in boosted kinematics relevant for LHC processes, in conjunction with cuts on the same-flavour lepton-pair masses. We demonstrated that the extraction of η_ℓ depends not only on the dressing radius but also on the production mechanism and the kinematic configuration of the Z boson. This highlights the need for a process- and setup-specific determination of η_ℓ when applying QT in realistic collider environments.

Third, we applied our refined prescription to inclusive ZZ production at the LHC and showed that QT and the helicity-amplitude (HA) approach yield results in excellent agreement when consistently using the NLO-corrected value of η_ℓ. Full off-shell effects, while present, were found to have only a mild numerical impact under typical fiducial selections.

Finally, we studied Higgs-boson decays to four leptons. For a Standard Model Higgs with $M_{\rm H} \simeq 125\,\text{GeV}$, the off-shell effects in the $\mathrm{H} \to \mathrm{ZZ}^* \to 4\ell$ channel prevent the straightforward application of the same prescription. Conversely, for a heavy Higgs boson ($M_{\rm H} \gg 2M_{\rm Z}$), the approach remains valid and we quantified the impact of formally higher-order (NNLO EW) effects, confirming their relevance in precision studies. This implies that order $\mathcal{O}(\alpha_{\rm ew}^2)$ effects have to be taken into account when spin-density-matrix coefficients are extracted from data.

JHEP02(2026)056

Our results establish a robust and general framework for performing quantum tomography at NLO EW accuracy for any process involving one or more *on-shell* Z bosons. EW higher-order effects can be sizeable and have to be taken into account: the proper extraction of spin-correlation coefficients that involves the spin-analysing power η_ℓ must be performed using its NLO EW prediction, possibly taking into account, via the HA method, the effects of cuts on the Z decay products.

We stress that the relevance of our findings does not pertain uniquely the measurement of quantum-entanglement and Bell-non-locality markers, but in general the sound determination of the spin-density matrix of any $\mathrm{Z} + X$ system, with the Z boson decaying into charged leptons. The results of this work provide clear guidance for upcoming experimental analyses both at the LHC and at future $\mathrm{e}^+\mathrm{e}^-$ facilities, where the clean experimental environment and high luminosity will allow measurements with unprecedented accuracy. Looking forward, the extension of this study to mixed QCD-EW corrections, to parton-shower effects, and to multi-boson final states will be essential to fully exploit quantum-inspired measurements at high-energy colliders, both within and beyond the SM.

Acknowledgments

The authors acknowledge support from the European Union (EU) COMETA COST Action (CA22130). GP acknowledges financial support from the EU Horizon Europe research and innovation programme under the Marie-Skłodowska Curie Action (MSCA) "POEBLITA — POlarised Electroweak Bosons at the LHC with Improved Theoretical Accuracy" — grant agreement Nr. 101149251 (CUP H45E2300129000) and the Italian Ministry of University and Research (MUR), with EU funds (NextGenerationEU), through the PRIN2022 grant agreement Nr. 20229KEFAM (CUP H53D23000980006). FF acknowledges financial support from the EU Horizon Europe research and innovation programme under the MSCA "QUANTUMLHC — Exploring quantum observables at the LHC" — grant agreement Nr. 101107121 (CUP J33C23001080006). MG is supported by CERN through the CERN Quantum Technology Initiative. DP acknowledges the financial support by the MUR, with NextGenerationEU funds, through the PRIN2022 grant Nr. 2022EZ3S3F; likewise FM, through the PRIN2022 grant Nr. 2022RXEZCJ, and by the project "QIHEP — Exploring the foundations of quantum information in particle physics", which is financed through the PNRR with NextGenerationEU funds, in the context of the extended partnership PE00000023 NQSTI (CUP J33C24001210007).

A Irreducible spin-1 tensor representations

The explicit form of the T_{lm} matrices introduced in eq. (2.7) reads [7, 23]

$$
\begin{aligned}
T_{11} &= \sqrt{\frac{3}{2}}\begin{pmatrix} 0 & -1 & 0 \\ 0 & 0 & -1 \\ 0 & 0 & 0 \end{pmatrix}, \qquad T_{10} = \sqrt{\frac{3}{2}}\begin{pmatrix} 1 & 0 & 0 \\ 0 & 0 & 0 \\ 0 & 0 & -1 \end{pmatrix}, \\
T_{22} &= \sqrt{3}\begin{pmatrix} 0 & 0 & 1 \\ 0 & 0 & 0 \\ 0 & 0 & 0 \end{pmatrix}, \qquad T_{21} = \sqrt{\frac{3}{2}}\begin{pmatrix} 0 & -1 & 0 \\ 0 & 0 & 1 \\ 0 & 0 & 0 \end{pmatrix}, \qquad T_{20} = \frac{1}{\sqrt{2}}\begin{pmatrix} 1 & 0 & 0 \\ 0 & -2 & 0 \\ 0 & 0 & 1 \end{pmatrix},
\end{aligned} \tag{A.1}
$$

with $T_{l,-m} = (-1)^m T^\dagger_{lm}$.

Data Availability Statement. This article has no associated data or the data will not be deposited.

Code Availability Statement. This article has no associated code or the code will not be deposited.

References

[1] A.J. Barr et al., *Quantum entanglement and Bell inequality violation at colliders*, *Prog. Part. Nucl. Phys.* **139** (2024) 104134 [arXiv:2402.07972] [INSPIRE].

[2] Y. Afik et al., *Quantum information meets high-energy physics: input to the update of the European strategy for particle physics*, *Eur. Phys. J. Plus* **140** (2025) 855 [arXiv:2504.00086] [INSPIRE].

[3] ATLAS collaboration, *Observation of quantum entanglement with top quarks at the ATLAS detector*, *Nature* **633** (2024) 542 [arXiv:2311.07288] [INSPIRE].

[4] CMS collaboration, *Observation of quantum entanglement in top quark pair production in proton–proton collisions at* $\sqrt{s} = 13$ *TeV*, *Rept. Prog. Phys.* **87** (2024) 117801 [arXiv:2406.03976] [INSPIRE].

[5] CMS collaboration, *Measurements of polarization and spin correlation and observation of entanglement in top quark pairs using lepton+jets events from proton-proton collisions at* $\sqrt{s} = 13$ *TeV*, *Phys. Rev. D* **110** (2024) 112016 [arXiv:2409.11067] [INSPIRE].

[6] A.J. Barr, *Testing Bell inequalities in Higgs boson decays*, *Phys. Lett. B* **825** (2022) 136866 [arXiv:2106.01377] [INSPIRE].

[7] J.A. Aguilar-Saavedra, A. Bernal, J.A. Casas and J.M. Moreno, *Testing entanglement and Bell inequalities in* $H \to ZZ$, *Phys. Rev. D* **107** (2023) 016012 [arXiv:2209.13441] [INSPIRE].

[8] R. Ashby-Pickering, A.J. Barr and A. Wierzchucka, *Quantum state tomography, entanglement detection and Bell violation prospects in weak decays of massive particles*, *JHEP* **05** (2023) 020 [arXiv:2209.13990] [INSPIRE].

[9] J.A. Aguilar-Saavedra, *Laboratory-frame tests of quantum entanglement in* $H \to WW$, *Phys. Rev. D* **107** (2023) 076016 [arXiv:2209.14033] [INSPIRE].

[10] M. Fabbrichesi, R. Floreanini, E. Gabrielli and L. Marzola, *Bell inequalities and quantum entanglement in weak gauge boson production at the LHC and future colliders*, *Eur. Phys. J. C* **83** (2023) 823 [arXiv:2302.00683] [INSPIRE].

[11] M. Fabbrichesi, R. Floreanini, E. Gabrielli and L. Marzola, *Stringent bounds on* HWW *and* HZZ *anomalous couplings with quantum tomography at the LHC*, *JHEP* **09** (2023) 195 [arXiv:2304.02403] [INSPIRE].

[12] R. Aoude, E. Madge, F. Maltoni and L. Mantani, *Probing new physics through entanglement in diboson production*, *JHEP* **12** (2023) 017 [arXiv:2307.09675] [INSPIRE].

[13] A. Bernal, P. Caban and J. Rembieliński, *Entanglement and Bell inequalities violation in* $H \to ZZ$ *with anomalous coupling*, *Eur. Phys. J. C* **83** (2023) 1050 [arXiv:2307.13496] [INSPIRE].

JHEP02(2026)056

[14] F. Fabbri, J. Howarth and T. Maurin, *Isolating semi-leptonic $H \to WW^*$ decays for Bell inequality tests*, *Eur. Phys. J. C* **84** (2024) 20 [arXiv:2307.13783] [INSPIRE].

[15] R.A. Morales, *Exploring Bell inequalities and quantum entanglement in vector boson scattering*, *Eur. Phys. J. Plus* **138** (2023) 1157 [arXiv:2306.17247] [INSPIRE].

[16] A. Bernal, P. Caban and J. Rembieliński, *Entanglement and Bell inequality violation in vector diboson systems produced in decays of spin-0 particles*, *Sci. Rep.* **15** (2025) 23410 [arXiv:2405.16525] [INSPIRE].

[17] M. Grossi, G. Pelliccioli and A. Vicini, *From angular coefficients to quantum observables: a phenomenological appraisal in di-boson systems*, *JHEP* **12** (2024) 120 [arXiv:2409.16731] [INSPIRE].

[18] M. Sullivan, *Constraining new physics with $h \to VV$ tomography*, arXiv:2410.10980 [INSPIRE].

[19] Y. Wu et al., *Testing Bell inequalities and probing quantum entanglement at CEPC*, *Phys. Rev. D* **111** (2025) 036008 [arXiv:2410.17025] [INSPIRE].

[20] R. Grabarczyk, *An improved Bell-CHSH observable for gauge boson pairs*, arXiv:2410.18022 [INSPIRE].

[21] J.A. Aguilar-Saavedra, *$H \to ZZ$ as a double-slit experiment*, *Phys. Lett. B* **868** (2025) 139639 [arXiv:2411.13464] [INSPIRE].

[22] A. Subba, R.K. Singh and R.M. Godbole, *Looking into the quantum entanglement in $H \to ZZ^\star$ at LHC within SMEFT framework*, arXiv:2411.19171 [INSPIRE].

[23] M. Del Gratta et al., *Quantum properties of $H \to VV^*$: precise predictions in the SM and sensitivity to new physics*, *JHEP* **09** (2025) 013 [arXiv:2504.03841] [INSPIRE].

[24] R. Ding et al., *Quantum entanglement between gauge boson pairs at a muon collider*, arXiv:2504.09832 [INSPIRE].

[25] J.A. Aguilar-Saavedra, *Quantum tomography beyond the leading order*, *Eur. Phys. J. C* **85** (2025) 969 [arXiv:2505.11870] [INSPIRE].

[26] D. Gonçalves, A. Kaladharan, F. Krauss and A. Navarro, *Quantum entanglement is quantum: ZZ production at the LHC*, *JHEP* **12** (2025) 122 [arXiv:2505.12125] [INSPIRE].

[27] A. Ruzi, Y. Wu, R. Ding and Q. Li, *Searching quantum entanglement in the $pp \to ZZ$ process*, *Chin. Phys.* **50** (2026) 023103 [arXiv:2506.16077] [INSPIRE].

[28] D. Gonçalves, A. Kaladharan and A. Navarro, *Higher-order corrections to quantum observables in $h \to WW^*$*, *JHEP* **11** (2025) 158 [arXiv:2506.19951] [INSPIRE].

[29] D.C. Kennedy and B.W. Lynn, *Electroweak radiative corrections with an effective Lagrangian: four fermion processes*, *Nucl. Phys. B* **322** (1989) 1 [INSPIRE].

[30] F.M. Renard and C. Verzegnassi, *A Z peak subtracted representation of four fermion processes at future e^+e^- colliders*, *Phys. Rev. D* **52** (1995) 1369 [INSPIRE].

[31] A. Ferroglia, G. Ossola and A. Sirlin, *Scale independent calculation of $\sin^2\theta_{\rm eff}^{\rm lept}$*, *Phys. Lett. B* **507** (2001) 147 [hep-ph/0103001] [INSPIRE].

[32] A. Ferroglia, G. Ossola, M. Passera and A. Sirlin, *Simple formulae for $\sin^2\theta_{\rm eff}^{\rm lept}$, M_W, Γ_l, and their physical applications*, *Phys. Rev. D* **65** (2002) 113002 [hep-ph/0203224] [INSPIRE].

[33] M. Chiesa, F. Piccinini and A. Vicini, *Direct determination of $\sin^2\theta_{\rm eff}^{\ell}$ at hadron colliders*, *Phys. Rev. D* **100** (2019) 071302 [arXiv:1906.11569] [INSPIRE].

[34] S. Amoroso et al., *Probing the weak mixing angle at high energies at the LHC and HL-LHC*, *Phys. Lett. B* **844** (2023) 138103 [arXiv:2302.10782] [INSPIRE].

[35] A. Biekötter, B.D. Pecjak and T. Smith, *Using the effective weak mixing angle as an input parameter in SMEFT*, *JHEP* **04** (2024) 073 [arXiv:2312.08446] [INSPIRE].

JHEP02(2026)056

[36] M. Chiesa, C.L. Del Pio and F. Piccinini, *On electroweak corrections to neutral current Drell–Yan with the POWHEG BOX*, *Eur. Phys. J. C* **84** (2024) 539 [arXiv:2402.14659] [INSPIRE].

[37] ATLAS collaboration, *Measurement of $W^{\pm}Z$ production cross sections and gauge boson polarisation in pp collisions at $\sqrt{s} = 13$ TeV with the ATLAS detector*, *Eur. Phys. J. C* **79** (2019) 535 [arXiv:1902.05759] [INSPIRE].

[38] F. Boudjema and R.K. Singh, *A model independent spin analysis of fundamental particles using azimuthal asymmetries*, *JHEP* **07** (2009) 028 [arXiv:0903.4705] [INSPIRE].

[39] R. Rahaman and R.K. Singh, *Breaking down the entire spectrum of spin correlations of a pair of particles involving fermions and gauge bosons*, *Nucl. Phys. B* **984** (2022) 115984 [arXiv:2109.09345] [INSPIRE].

[40] ALEPH et al. collaborations, *Precision electroweak measurements on the Z resonance*, *Phys. Rept.* **427** (2006) 257 [hep-ex/0509008] [INSPIRE].

[41] A. Denner and G. Pelliccioli, *Polarized electroweak bosons in W^+W^- production at the LHC including NLO QCD effects*, *JHEP* **09** (2020) 164 [arXiv:2006.14867] [INSPIRE].

[42] A. Ballestrero, E. Maina and G. Pelliccioli, *W boson polarization in vector boson scattering at the LHC*, *JHEP* **03** (2018) 170 [arXiv:1710.09339] [INSPIRE].

[43] A. Ballestrero, E. Maina and G. Pelliccioli, *Polarized vector boson scattering in the fully leptonic WZ and ZZ channels at the LHC*, *JHEP* **09** (2019) 087 [arXiv:1907.04722] [INSPIRE].

[44] A. Ballestrero, E. Maina and G. Pelliccioli, *Different polarization definitions in same-sign WW scattering at the LHC*, *Phys. Lett. B* **811** (2020) 135856 [arXiv:2007.07133] [INSPIRE].

[45] A. Denner and G. Pelliccioli, *NLO QCD predictions for doubly-polarized WZ production at the LHC*, *Phys. Lett. B* **814** (2021) 136107 [arXiv:2010.07149] [INSPIRE].

[46] R. Poncelet and A. Popescu, *NNLO QCD study of polarised W^+W^- production at the LHC*, *JHEP* **07** (2021) 023 [arXiv:2102.13583] [INSPIRE].

[47] A. Denner and G. Pelliccioli, *NLO EW and QCD corrections to polarized ZZ production in the four-charged-lepton channel at the LHC*, *JHEP* **10** (2021) 097 [arXiv:2107.06579] [INSPIRE].

[48] D.N. Le and J. Baglio, *Doubly-polarized WZ hadronic cross sections at NLO QCD + EW accuracy*, *Eur. Phys. J. C* **82** (2022) 917 [arXiv:2203.01470] [INSPIRE].

[49] D.N. Le, J. Baglio and T.N. Dao, *Doubly-polarized WZ hadronic production at NLO QCD+EW: calculation method and further results*, *Eur. Phys. J. C* **82** (2022) 1103 [arXiv:2208.09232] [INSPIRE].

[50] A. Denner, C. Haitz and G. Pelliccioli, *NLO QCD corrections to polarized diboson production in semileptonic final states*, *Phys. Rev. D* **107** (2023) 053004 [arXiv:2211.09040] [INSPIRE].

[51] T.N. Dao and D.N. Le, *Enhancing the doubly-longitudinal polarization in WZ production at the LHC*, *Commun. in Phys.* **33** (2023) 223 [arXiv:2302.03324] [INSPIRE].

[52] G. Pelliccioli and G. Zanderighi, *Polarised-boson pairs at the LHC with NLOPS accuracy*, *Eur. Phys. J. C* **84** (2024) 16 [arXiv:2311.05220] [INSPIRE].

[53] A. Denner, C. Haitz and G. Pelliccioli, *NLO EW corrections to polarised W^+W^- production and decay at the LHC*, *Phys. Lett. B* **850** (2024) 138539 [arXiv:2311.16031] [INSPIRE].

[54] T.N. Dao and D.N. Le, *NLO electroweak corrections to doubly-polarized W^+W^- production at the LHC*, *Eur. Phys. J. C* **84** (2024) 244 [arXiv:2311.17027] [INSPIRE].

[55] A. Denner, C. Haitz and G. Pelliccioli, *NLO EW and QCD corrections to polarised same-sign WW scattering at the LHC*, *JHEP* **11** (2024) 115 [arXiv:2409.03620] [INSPIRE].

[56] T.N. Dao and D.N. Le, *Polarized W^+W^- pairs at the LHC: effects from bottom-quark induced processes at NLO QCD + EW*, *Eur. Phys. J. C* **85** (2025) 108 [arXiv:2409.06396] [INSPIRE].

JHEP02(2026)056

[57] U. Haisch et al., *Polarized-boson pairs at NLO in the SMEFT*, *JHEP* **11** (2025) 080 [arXiv:2507.21768] [INSPIRE].

[58] P. Richardson, *Spin correlations in Monte Carlo simulations*, *JHEP* **11** (2001) 029 [hep-ph/0110108] [INSPIRE].

[59] P. Artoisenet, R. Frederix, O. Mattelaer and R. Rietkerk, *Automatic spin-entangled decays of heavy resonances in Monte Carlo simulations*, *JHEP* **03** (2013) 015 [arXiv:1212.3460] [INSPIRE].

[60] D. Buarque Franzosi, O. Mattelaer, R. Ruiz and S. Shil, *Automated predictions from polarized matrix elements*, *JHEP* **04** (2020) 082 [arXiv:1912.01725] [INSPIRE].

[61] M. Pellen, R. Poncelet and A. Popescu, *Polarised $W + j$ production at the LHC: a study at NNLO QCD accuracy*, *JHEP* **02** (2022) 160 [arXiv:2109.14336] [INSPIRE].

[62] M. Hoppe, M. Schönherr and F. Siegert, *Polarised cross sections for vector boson production with Sherpa*, *JHEP* **04** (2024) 001 [arXiv:2310.14803] [INSPIRE].

[63] C. Carrivale et al., *Precise standard-model predictions for polarised Z-boson pair production and decay at the LHC*, *Eur. Phys. J. C* **85** (2025) 1342 [arXiv:2505.09686] [INSPIRE].

[64] CMS collaboration, *Measurements of production cross sections of polarized same-sign W boson pairs in association with two jets in proton-proton collisions at $\sqrt{s} = 13$ TeV*, *Phys. Lett. B* **812** (2021) 136018 [arXiv:2009.09429] [INSPIRE].

[65] CMS collaboration, *Measurement of the inclusive and differential WZ production cross sections, polarization angles, and triple gauge couplings in pp collisions at $\sqrt{s} = 13$ TeV*, *JHEP* **07** (2022) 032 [arXiv:2110.11231] [INSPIRE].

[66] ATLAS collaboration, *Observation of gauge boson joint-polarisation states in $W^{\pm}Z$ production from pp collisions at $\sqrt{s} = 13$ TeV with the ATLAS detector*, *Phys. Lett. B* **843** (2023) 137895 [arXiv:2211.09435] [INSPIRE].

[67] ATLAS collaboration, *Evidence of pair production of longitudinally polarised vector bosons and study of CP properties in $ZZ \to 4\ell$ events with the ATLAS detector at $\sqrt{s} = 13$ TeV*, *JHEP* **12** (2023) 107 [arXiv:2310.04350] [INSPIRE].

[68] ATLAS collaboration, *Studies of the energy dependence of diboson polarization fractions and the radiation-amplitude-zero effect in WZ production with the ATLAS detector*, *Phys. Rev. Lett.* **133** (2024) 101802 [*Erratum ibid.* **133** (2024) 169901] [arXiv:2402.16365] [INSPIRE].

[69] ATLAS collaboration, *Evidence for longitudinally polarized W bosons in the electroweak production of same-sign W boson pairs in association with two jets in pp collisions at $\sqrt{s} = 13$ TeV with the ATLAS detector*, *Phys. Rev. Lett.* **135** (2025) 111802 [arXiv:2503.11317] [INSPIRE].

[70] J. Alwall et al., *The automated computation of tree-level and next-to-leading order differential cross sections, and their matching to parton shower simulations*, *JHEP* **07** (2014) 079 [arXiv:1405.0301] [INSPIRE].

[71] R. Frederix et al., *The automation of next-to-leading order electroweak calculations*, *JHEP* **11** (2018) 085 [*Erratum ibid.* **11** (2021) 085] [arXiv:1804.10017] [INSPIRE].

[72] S. Actis et al., *RECOLA: REcursive Computation of One-Loop Amplitudes*, *Comput. Phys. Commun.* **214** (2017) 140 [arXiv:1605.01090] [INSPIRE].

[73] A. Denner, S. Dittmaier and L. Hofer, *Collier: a fortran-based Complex One-Loop LIbrary in Extended Regularizations*, *Comput. Phys. Commun.* **212** (2017) 220 [arXiv:1604.06792] [INSPIRE].

[74] J. Baglio et al., *Release note: VBFNLO 3.0*, *Eur. Phys. J. C* **84** (2024) 1003 [arXiv:2405.06990] [INSPIRE].

JHEP02(2026)056

[75] S. Frixione, Z. Kunszt and A. Signer, *Three jet cross-sections to next-to-leading order*, *Nucl. Phys. B* **467** (1996) 399 [hep-ph/9512328] [INSPIRE].

[76] PARTICLE DATA GROUP collaboration, *Review of particle physics*, *Phys. Rev. D* **110** (2024) 030001 [INSPIRE].

[77] A. Sirlin, *Radiative corrections in the $SU(2)_L \times U(1)$ theory: a simple renormalization framework*, *Phys. Rev. D* **22** (1980) 971 [INSPIRE].

[78] A. Denner, S. Dittmaier, M. Roth and D. Wackeroth, *Electroweak radiative corrections to $e^+e^- \to WW \to 4$ fermions in double pole approximation: the RACOONWW approach*, *Nucl. Phys. B* **587** (2000) 67 [hep-ph/0006307] [INSPIRE].

[79] S. Kallweit et al., *NLO QCD+EW predictions for V + jets including off-shell vector-boson decays and multijet merging*, *JHEP* **04** (2016) 021 [arXiv:1511.08692] [INSPIRE].

[80] S. Dittmaier, *A general approach to photon radiation off fermions*, *Nucl. Phys. B* **565** (2000) 69 [hep-ph/9904440] [INSPIRE].

[81] L. Chen and A. Freitas, *GRIFFIN: a C++ library for electroweak radiative corrections in fermion scattering and decay processes*, *SciPost Phys. Codeb.* **2023** (2023) 18 [arXiv:2211.16272] [INSPIRE].

[82] D.Y. Bardin, A. Leike, T. Riemann and M. Sachwitz, *Energy dependent width effects in e^+e^- annihilation near the Z boson pole*, *Phys. Lett. B* **206** (1988) 539 [INSPIRE].

[83] A. Denner, S. Dittmaier, M. Roth and L.H. Wieders, *Electroweak corrections to charged-current $e^+e^- \to 4$ fermion processes: technical details and further results*, *Nucl. Phys. B* **724** (2005) 247 [*Erratum ibid.* **854** (2012) 504] [hep-ph/0505042] [INSPIRE].

[84] A. Denner and S. Dittmaier, *Electroweak radiative corrections for collider physics*, *Phys. Rept.* **864** (2020) 1 [arXiv:1912.06823] [INSPIRE].

[85] C.F. Uhlemann and N. Kauer, *Narrow-width approximation accuracy*, *Nucl. Phys. B* **814** (2009) 195 [arXiv:0807.4112] [INSPIRE].

[86] S. Catani and M.H. Seymour, *A general algorithm for calculating jet cross-sections in NLO QCD*, *Nucl. Phys. B* **485** (1997) 291 [*Erratum ibid.* **510** (1998) 503] [hep-ph/9605323] [INSPIRE].

[87] S. Catani, S. Dittmaier, M.H. Seymour and Z. Trocsanyi, *The dipole formalism for next-to-leading order QCD calculations with massive partons*, *Nucl. Phys. B* **627** (2002) 189 [hep-ph/0201036] [INSPIRE].

[88] M. Cacciari, G.P. Salam and G. Soyez, *The anti-k_t jet clustering algorithm*, *JHEP* **04** (2008) 063 [arXiv:0802.1189] [INSPIRE].

JHEP02(2026)056